Glycobiology vol. 16 no. 10 pp. 1007–1019, 2006
doi:10.1093/glycob/cwl023
Advance Access publication on July 21, 2006

# Down-regulation of trypsinogen expression is associated with growth retardation in α1,6-fucosyltransferase-deficient mice: attenuation of proteinase-activated receptor 2 activity

Wenzhe Li[1,3,8], Takatoshi Nakagawa[1,3,7], Nobuto Koyama[1,5,7], Xiangchun Wang[4], Jinhua Jin[4], Yoko Mizuno-Horikawa[4], Jianguo Gu[4,7], Eiji Miyoshi[4,7], Ikunoshin Kato[5], Koichi Honke[6], Naoyuki Taniguchi[4,8], and Akihiro Kondo[2,3,7,8]

[3]Department of Glycotherapeutics, [4]Department of Biochemistry, Osaka University Graduate School of Medicine, Osaka 565-0871; [5]Takara Bio Inc., Shiga 520-2193; [6]Department of Molecular Genetics, Kochi University Graduate School of Medicine, Kochi 783-8505, Japan; [7]CREST, JST, 4-1-8 Honcho Kawaguchi, Saitama, 332-0012; and [8]the 21st century COE program, Ministry of Education, Culture, Sports, Science and Technology, 2-5-1 Marunouchi, Chiyoda-ku, Tokyo 100-8959, Japan

*Received on June 1, 2006; revised on July 3, 2006; accepted on July 10, 2006*

**Alpha1,6-fucosyltransferase (*Fut8*) plays important roles in physiological and pathological conditions. *Fut8*-deficient (*Fut8*$^{-/-}$) mice exhibit growth retardation, earlier postnatal death, and emphysema-like phenotype. To investigate the underlying molecular mechanism by which growth retardation occurs, we examined the mRNA expression levels of *Fut8*$^{-/-}$ embryos (18.5 days postcoitum [dpc]) using a cDNA microarray. The DNA microarray and real-time polymerase chain reaction (PCR) analysis showed that a group of genes, including trypsinogens 4, 7, 8, 11, 16, and 20, were down-regulated in *Fut8*$^{-/-}$ embryos. Consistently, the expression of trypsinogen proteins was found to be lower in *Fut8*$^{-/-}$ mice in the duodenum, small intestine, and pancreas. Trypsin, an active form of trypsinogen, regulates cell growth through a G-protein-coupled receptor, the proteinase-activated receptor 2 (PAR-2). In a cell culture system, a *Fut8* knockdown mouse pancreatic acinar cell carcinoma, TGP49-*Fut8*-KDs, showed decreased growth rate, similar to that seen in *Fut8*$^{-/-}$ mice, and the decreased growth rate was rescued by the application of the PAR-2-activating peptide (SLIGRL-$NH_2$). Moreover, epidermal growth factor (EGF)-induced receptor phosphorylation was attenuated in TGP49-*Fut8*-KDs, which was highly associated with a reduction of trypsinogens mRNA levels. The addition of exogenous EGF recovered c-fos, c-jun, and trypsinogen mRNA expression in TGP49-*Fut8*-KDs. Again, the EGF-induced up-regulation of c-fos and c-jun mRNA expression was significantly blocked by the protein kinase C (PKC) inhibitor. Our findings clearly demonstrate a relationship between *Fut8* and the regulation of EGF receptor (EGFR)-trypsin-PAR-2 pathway in controlling cell growth and that the EGFR-trypsin-PAR-2 pathway is suppressed in TGP49-*Fut8*-KDs as well as in *Fut8*$^{-/-}$ mice.**

*Key words:* cell growth/*FUT8* knockdown cell/PAR-2/trypsinogen/α1,6-fucosyltransferase

## Introduction

*Fut8* transfers fucose to the innermost GlcNAc residue of complex *N*-glycans via α1,6-linkage (core fucosylation) in the Golgi apparatus in mammals (Wilson *et al.*, 1976). *Fut8*-deficient (*Fut8*$^{-/-}$) mice showed a dramatically changed phenotype similar to that of GDP-4-keto-6-deoxy-D-mannose epimerase–reductase (FX)-deficient (FX$^{-/-}$) mice (Smith *et al.*, 2002), showing a postnatal failure to thrive, and all the survivors manifested growth retardation (Wang *et al.*, 2005). In comparison with other terminal fucose-deficient mice such as *Fut1*$^{-/-}$ (Domino *et al.*, 2001), *Fut2*$^{-/-}$ (Domino *et al.*, 2001), *Fut7*$^{-/-}$ (Maly *et al.*, 1996), double *Fut4*$^{-/-}$/*Fut7*$^{-/-}$ (Homeister *et al.*, 2001), and *Fut9*$^{-/-}$ (Kudo *et al.*, 2004) mice, which develop normally and exhibit no gross phenotypic abnormalities, the phenotypes of the *Fut8*$^{-/-}$ mice were much severe in terms of development and growth.

It is well known that trypsinogen is synthesized by pancreas acinar cells and is secreted into the intestinal lumen after the ingestion of food, where it is processed to active trypsin by enterokinase. Although the function of trypsin is traditionally related to the digestion of consumed proteins, recent discoveries suggest that it also serves as an activator of the proteinase-activated receptor 2 (PAR-2), which, in turn, induces various biological effects, such as cell growth (Ossovskaya and Bunnett, 2004). Four members of the PAR family have been cloned to date: PAR-1, PAR-3, and PAR-4 can be activated by thrombin, whereas PAR-2 is activated by trypsin and mast cell tryptase but not by thrombin (Kahn *et al.*, 1998). PAR-2 is a seven transmembrane spanning G-protein-coupled receptor (Nystedt *et al.*, 1994) and is widely expressed in several tissues and cell lines. Digestive organs, such as pancreas and intestine, especially highly express PAR-2 (Bohm *et al.*, 1996; Ossovskaya and Bunnett, 2004). It has been reported that PAR-2 plays multiple physiological roles in various tissues such as ion transport, intestinal mobility, several exocrine secretion, and in the response of tissues to injury, including inflammation, pain, and healing (Ossovskaya and Bunnett,

[1]These authors contributed equally to the work.
[2]To whom correspondence should be addressed; e-mail: kondoa@glycot.med.osaka-u.ac.jp

© 2006 The Author(s)
This is an Open Access article distributed under the terms of the Creative Commons Attribution Non-Commercial License (http://creativecommons.org/licenses/by-nc/2.0/uk/) which permits unrestricted non-commercial use, distribution, and reproduction in any medium, provided the original work is properly cited.

2004). Indeed, 20% of all *PAR-2*$^{-/-}$ mice were either stillborn or died within 48 h of birth (Damiano *et al.*, 1999). Trypsin could cleave the extracellular N-terminus of mouse PAR-2, at $^{33}$SKGR*SLIGRL$^{42}$, exposing the tethered ligand domain SLIGRL, which then binds to conserved regions in the extracellular loop II of the cleaved receptor and triggers receptor function under physiological conditions (Nystedt *et al.*, 1994). A synthetic peptide corresponding to the tethered ligand sequences (SLIGRL) can also activate PAR-2 selectively and is an important tool for studying the functions of mouse PAR-2. Indeed, either trypsin or SLIGRL-$NH_2$ can stimulate the mitogen-activated protein kinase (MAPK) cascade and may regulate cell proliferation (Darmoul *et al.*, 2004; Ossovskaya and Bunnett, 2004).

The epidermal growth factor receptor (EGFR) consists of an extracellular domain, a hydrophobic transmembrane domain, and an intracellular domain (Carpenter and Cohen, 1990). It has been reported that glycosylation is a common posttranslational feature in EGFR, which contains 11 *N*-glycosylation sites but no *O*-linked oligosaccharides (Stroop *et al.*, 2000). Several researchers have reported that the *N*-glycosylation of EGFR is an important parameter in its ligand-binding activity (Pratt and Pastan, 1978; Soderquist and Carpenter, 1984; Rebbaa *et al.*, 1997; Tsuda *et al.*, 2000; Guo *et al.*, 2004). Moreover, Stroop and others (2000) reported that the complex-type oligosaccharides linked to EGFR have di-, tri-, and tetra-antennary structures with core fucosylation. Wang and others (2005) reported that the binding affinity of the transforming growth factor-β (TGF-β) toward TGF-β type II receptor is diminished in *Fut8*$^{-/-}$ mouse embryonic fibroblasts as well as in *Fut8*$^{-/-}$ mice. It is conceivable that core fucose residues of *N*-glycans associated with EGFR may modify its receptor function, such as ligand–receptor binding, dimerization, and phosphorylation.

Because 70% of *Fut8*$^{-/-}$ mice showed an earlier postnatal death, sophisticated methods were needed to study the functions of *Fut8*. Short interfering RNAs (siRNAs) is a powerful new tool for analyzing gene knockdown phenotypes in living mammalian cells (Elbashir *et al.*, 2001). To determine the underlying mechanism of the growth retardation seen in *Fut8*$^{-/-}$ mice, we established a *Fut8* knockdown cell line by a siRNA technique using mouse pancreatic acinar cell carcinoma (TGP49). The *Fut8* knockdown cells provided a good model for studying relationships among *Fut8*, trypsinogens, and growth retardation. We demonstrate here that core fucosylation of *N*-glycans on EGFR regulates cell proliferation by EGFR-trypsin-PAR-2 signaling.

## Results

### *Trypsinogen genes were down-regulated in* Fut8$^{-/-}$ *mice*

The DNA microarray enables the simultaneous measurement and comparison of the expression levels of thousands of genes and has great advantages in investigating complex gene expression patterns aimed at the discovery of novel molecular functions (Schena *et al.*, 1995). To elucidate the underlying mechanism of growth retardation, mRNA expression profiles of *Fut8*$^{+/+}$ versus *Fut8*$^{-/-}$ embryos were compared using an IntelliGene II mouse DNA Chip. We found 37 genes that showed more than 2-fold changes in their expressions between *Fut8*$^{+/+}$ and *Fut8*$^{-/-}$ embryos (18.5 days postcoitum [dpc]). Among these genes, 23 were up-regulated and 14 were down-regulated in *Fut8*$^{-/-}$ mice (Supplemental Table IA and B). It is particularly noteworthy that five trypsinogens 4, 7, 8, 11, and 16 were found in grouped genes, expressions of which were lower in *Fut8*$^{-/-}$ mice (Table I). Twenty mouse trypsinogen genes were located on chromosome 6, trypsinogens 1–20 (GeneBank accession number AE000663, AE000664, AE000665), of which 11 (trypsinogens 4, 5, 7, 8, 9, 10, 11, 12, 15, 16, and 20) are thought to be transcribed into RNA, seven (trypsinogens 1, 3, 13, 14, 17, 18, and 19) are pseudogenes, and two (trypsinogens 2 and 6) are relic genes. The trypsinogens 11 and 8 corresponded to trypsin 3 and 4 on the DNA chip, respectively. The mRNA expressions of trypsinogens 8, 11, and 16 on this DNA chip showed 3.2-, 4.6-, and 5.6-fold reductions, respectively. The trypsinogens 4 and 7 corresponded to RIKEN cDNA 1810009J06 gene (NM_023707) and RIKEN cDNA 2210010C04 gene (NM_023333) on this DNA chip, respectively. The mRNA expression of trypsinogens 4 and 7 showed 3.6- and 7.0-fold reduction in *Fut8*$^{-/-}$ mice, respectively. The microarray data were then validated by real-time polymerase chain reaction (PCR). The expression levels of several trypsinogens were similar to those observed in the DNA microarry analysis (Table I). Moreover, the expression of trypsinogen 20 (mouse pancreatic trypsin), which is thought to be involved in food digestion, proteolysis, peptidolysis, and hydrolytic activity in the mouse, showed a 4.9-fold reduction by the specific real-time PCR primers for trypsinogen 20 (Table II). Indeed, the cDNA sequence of trypsinogen 20 shared a high degree of identity (67, 74, 91, 88, and 89%) with trypsinogens 4, 7, 8, 11, and 16, respectively.

Trypsinogen proteins in tissue homogenates from the duodenum, small intestine, and pancreas were detected by western blot analysis. The expression of the trypsinogens was significantly lower in *Fut8*$^{-/-}$ mice than in *Fut8*$^{+/+}$ mice (Figure 1A). The trypsinogens bands represented the autolytically cleaved so-called two-chain form. In addition, gelatin zymography also showed a reduction of trypsin in *Fut8*$^{-/-}$ mice (data not shown). Indeed, the pancreas tissues express core fucosylated *N*-glycans, as confirmed by fucose lectin, *Aspergillus oryzae* lectin (AOL). Immunostaining of the pancreas specimens with anti-trypsinogen immunoglobulin (Ig)G also showed a lower expression of trypsinogens in *Fut8*$^{-/-}$ mice, compared with *Fut8*$^{+/+}$ mice (Figure 1B). Collectively, these results suggest that the core fucosylation of *N*-glycans correlates with trypsinogen expressions and gene deletion of *Fut8* results in the reduction of trypsinogen expression at both the mRNA and protein levels.

### *Loss of* Fut8 *induced the down-regulation of trypsinogen expression in TGP49 cells*

To clarify the association of *Fut8* with trypsinogen expression, we attempted to knockdown *Fut8* using siRNA in TGP49 cells (Pettengill *et al.*, 1994). First, we designed specific *Fut8*-siRNA fragments complementary to different regions of *Fut8* Open Reading Frame to observe the knockdown efficiency of *Fut8*. The sequences of the siRNA correspond to nucleotides 1016–1034 (No. 2), 2302–2320 (No. 5), 918–936 (No.8), and 1386–1404 (No.16) of mouse *Fut8* (NM_016893). Among the four siRNA fragments, siRNA

**Table I.** Schematic representation of the fold changes of the mRNAs expression of several trypsinogens in Fut8–/– mice

| Gene name | GenBank access number | Fold change average ($FUT8^{-/-}$ mice/$FUT8^{+/+}$ mice) | |
|---|---|---|---|
| | | DNA microarray[a] | Real-time PCR[b] |
| Trypsinogen 4 (RIKEN cDNA 1810009J06 gene) | NM_023707 | 0.28 | — |
| Trypsinogen 7 (RIKEN cDNA_2210010C04 gene) | NM_023333 | 0.14 | 0.18 |
| Trypsinogen 8 (Trypsin 4) | NM_011646 | 0.31 | 0.43 |
| Trypsinogen 11 (Trypsin 3) | NM_011645 | 0.22 | 0.12 |
| Trypsinogen 16 | NM_053243 | 0.18 | 0.17 |
| Trypsinogen 20 | NM_009430 | — | 0.20 |

[a]Values are means of cy dye swapping ($N = 2$).
[b]Values are means of triple independent experiments.

**Table II.** Primer sequences used in real-time PCR

| Gene name | Gene bank access number | Direction | Sequence |
|---|---|---|---|
| FUT8 | NM_016893 | Forward | 5′-AACAGCTTGTTAAGGCCAAAG-3′ |
| | | Reverse | 5′-GCATGTCTTTGGAGTTCATTTC-3′ |
| Trypsinogen 7 | NM_023333 | Forward | 5′-GCCACAGTGAGCAACCATGAA-3′ |
| | | Reverse | 5′-CTGGCAGGTGTAGCCTCCAA-3′ |
| Trypsinogen 8 | NM_011646 | Forward | 5′-CTTGAGCTTTGGTGTGAAC-3′ |
| | | Reverse | 5′-CAACACAGATCATGTTATTG-3′ |
| Trypsinogen 11 | NM_011645 | Forward | 5′-TCTTAGCTTTGGTGTCAGTG-3′ |
| | | Reverse | 5′-AGCACAGACCATGTTACCAG-3′ |
| Trypsinogen 16 | NM_053243 | Forward | 5′-CTGTGACCCTCAATGCCAGA-3′ |
| | | Reverse | 5′-TCCCAGGATAGGAAGCCTCA-3′ |
| Trypsinogen 20 | NM_009430 | Forward | 5′-GCCAGAGTGGCCTCTGTAC-3′ |
| | | Reverse | 5′-CAGCACTGGGGCATCAACA-3′ |
| c-fos | NM_010234 | Forward | 5′-CGGGTTTCAACGCCGACTAC-3′ |
| | | Reverse | 5′-AAAGTTGGCACTAGAGACGGACAGA-3′ |
| c-jun | NM_010591 | Forward | 5′-CTGTATGAAGTGGCATGTGCTGTG-3′ |
| | | Reverse | 5′-CCCTGCTTTGAGAATCAACAGCTAA-3′ |
| GnT III | NM_010795 | Forward | 5′-TCAAGCCATCAACATCAAC-3′ |
| | | Reverse | 5′-GTGGCGGATGTACTCGAAGG-3′ |
| β4GalT-I | NM_022305 | Forward | 5′-CAGCGCCAGCAACTCGACTA-3′ |
| | | Reverse | 5′-TCGATTGAACATGGTGTCTCCAG-3′ |
| GAPDH | NM_001001303 | Forward | 5′-AAATGGTGAAGGTCGGTGTG-3′ |
| | | Reverse | 5′-TGAAGGGGTCGTTGATGG-3′ |

(No. 16) was the strongest inhibitor of the *Fut8* expression, suppressing about 50% of the FUT8 activity, and this effect was not long lasting (data not shown).

It is important to assess the role of *Fut8* under conditions where the effect of endogenous *Fut8* is completely eliminated. To stably silence *Fut8* expression, we designed a retrovirus expression system using a pSINsi-mU6 cassette vector inserted with *Fut8* siRNA (No. 16) and established stable *Fut8* knockdown cell lines, referred to as TGP49-*Fut8*-KD1 and TGP49-*Fut8*-KD2. As shown in Figure 2A, B, and C, the introduction of *Fut8* siRNA almost completely suppressed *Fut8* expression. The *Fut8* mRNA expressions were reduced to 4.9 and 2.1% of the control in TGP49-*Fut8*-KD1 and TGP49-*Fut8*-KD2, respectively (Figure 2A). No apparent changes were found in the expressions of other glycosyltransferase genes, such as *N*-acetylglucosaminyltransferase III (GnT III) and β1, 4-galactosyltransferase I (β4GalT-I), suggesting that there is no off-target effect in this system (Supplemental Figure 1). FUT8 activities were barely detectable in TGP49-*Fut8*-KD1 and TGP49-*Fut8*-KD2 (Figure 2B). If any, the FUT8 activities of TGP49-*Fut8*-KDs were less than 5% of those of TGP49-*Fut8*-WT (759.1 pmol/h/mg) as well. Again, an *Aleuria aurantia* lectin (AAL) blot analysis reflected the results of the mRNA expressions and enzyme activities (Figure 2C). In TGP49-*Fut8*-KDs, the expression of trypsinogen proteins and mRNA was also reduced (Figure 2D and E). A sequence analysis of the trypsinogen cDNA cut

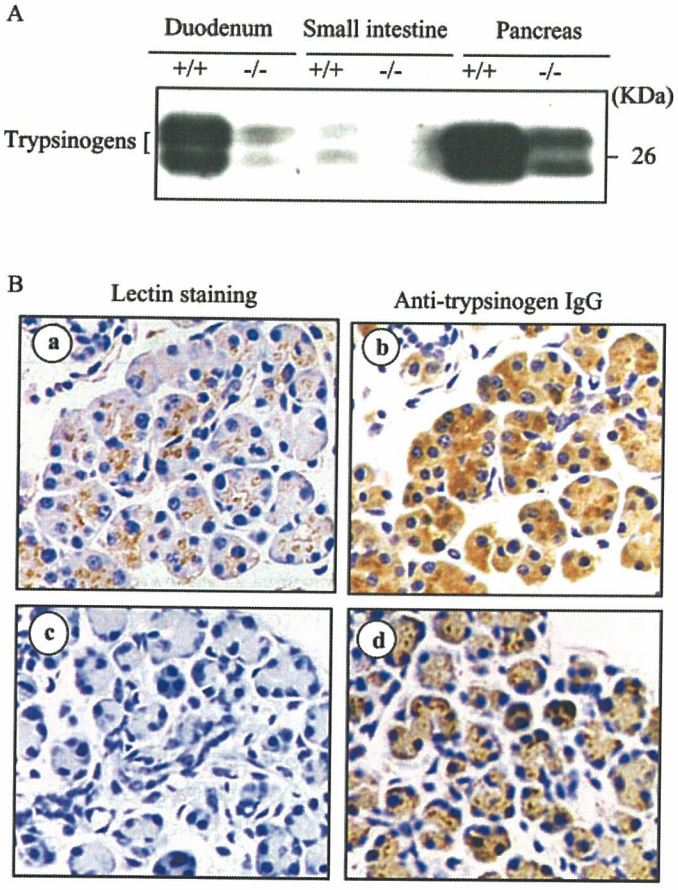


**Fig. 1.** Reduction of trypsinogen expression in extracts of *Fut8*$^{-/-}$ mice tissues (4 days old). Protein extracts were prepared from the indicated tissues, as described in *Materials and methods*, and appropriate amounts of each fraction were then mixed with 4× Laemmli loading buffer, and the proteins were resolved in 12.5% SDS–PAGE. The amount of protein loaded on the gel was 20 μg for the duodenum, 20 μg for small intestine, and 20 ng for pancreas. (**A**) Western blots of trypsinogens protein expression using rabbit anti-bovine trypsinogen IgG. (**B**) Immunohistochemical localization of core fucosylation molecules and trypsinogens in pancreas tissues (4 days old). The sections from 4-day-old mice were stained with AOL and anti-trypsinogen IgG. Panels a and c indicate pancreatic tissue of *Fut8*$^{+/+}$ and *Fut8*$^{-/-}$ mice stained with AOL; Panels b and d indicate pancreases of *Fut8*$^{+/+}$ and *Fut8*$^{-/-}$ mice stained by anti-trypsinogen IgG. Arrowheads: positive staining for trypsinogen and core fucosylated molecules. Experimental conditions are described in *Materials and methods*. Magnification is 100×.

from the gel showed that its cDNA sequence completely matched with trypsinogen 20 in GeneBank (NM_009430) (data not shown). It is conceivable that introducing siRNA resulted in the elimination of *Fut8* expression, followed by the down-regulation of trypsinogens expression in TGP49-*Fut8*-KDs.

### Fut8 *ablation led to the reduced proliferation, and it is rescued by the application of PAR-2 agonist, SLIGRL-NH$_2$*

The growth rates of TGP49-*Fut8*-KDs were much slower than those of TGP49-*Fut8*-WT, resembling the growth retardation of *Fut8*$^{-/-}$ mice (Figure 3). Cell confluence was reached between days 2 and 3 for TGP49-*Fut8*-WT and between days 4 and 5 for TGP49-*Fut8*-KDs. Trypsin has been shown to play a role in regulating cell growth by interacting with PAR-2 in addition to its role in digestion. In pancreatic cancer cells, trypsinogens were reported to be activated into trypsin by urokinase-type plasminogen activator (uPA) (Uchima *et al.*, 2003). We detected uPA in TGP49-derived cell culture supernatants by western blot and gelatin zymograms (Supplemental Figure 2 and data not shown). TGP49-*Fut8*-WT and TGP49-*Fut8*-KDs expressed comparable levels of PAR-2, as detected by western blots and immunocytochemical analysis (Figure 4A and B). Bands at about 55 kDa corresponding to the known molecular mass of PAR-2 were visualized by western blot analysis (Figure 4A). In addition, an analysis of PAR-2 localization by confocal microscopy demonstrated that the PAR-2 expression of TGP49-*Fut8*-KD1 was, similar to TGP49-*Fut8*-WT, localized mainly on the plasma membrane (Figure 4B). PAR-2 contains two sites for *N*-linked glycosylation at Asn$^{30}$, in proximity to the activation site in the extracellular tail, and at Asn$^{222}$ in the extracellular loop II of PAR-2. In contrast to TGP49-*Fut8*-WT, the core fucosylation of TGP49-*Fut8*-KDs was barely detectable by AOL staining (Figure 4C). These results suggest that the core fucosylation of PAR-2 does not affect its stability and cell surface expression.

SLIGRL-NH$_2$ is a well-known and useful probe for assessing the biological role of PAR-2. Shimamoto and others (2004) reported that SLIGRL-NH$_2$ stimulates cell proliferation through PAR-2 in pancreatic cancer cells. Here, the effect of SLIGRL-NH$_2$ treatment on cell growth was studied in TGP49-derivative cells. The proliferation of TGP49-*Fut8*-KDs was stimulated by 25 and 50 μg/mL of SLIGRL-NH$_2$, and stimulation by 25 μg/mL of SLIGRL-NH$_2$ evoked a cell growth rate comparable to the control level (Figure 5). The blockade of PAR-2 with 5 μg/mL of anti-PAR-2 antibody completely prevented SLIGRL-NH$_2$-mediated cell proliferation, indicating the crucial role of PAR-2 in cell proliferation (Figure 5). Moreover, in comparison with TGP49-*Fut8*-KDs, 30~40% of the cell growth of TGP49-*Fut8*-WT was suppressed by application of 5 μg/mL of the anti-PAR-2 antibody (Figure 3), indicating that the growth of TGP49 cells is partially dependent on PAR-2 stimulation in an autocrine manner. These findings clearly show that the reduced trypsinogen in *Fut8*$^{-/-}$ mice and/or in TGP49-*Fut8*-KDs are directly associated with cell growth control, at least in part, through the PAR-2 pathway.

### *Attenuation of EGF-induced EGFR phosphorylation led to down-regulation of trypsinogen expression*

Because it has been reported that 12-*O*-tetradecanoylphorbol-13-acetate (TPA) induces trypsinogen expression in endothelial cells (Koshikawa *et al.*, 1997), we suspected that protein kinase C (PKC) signaling could be involved in the trypsinogen reduction in TGP49-*Fut8*-KDs. PKC is activated by many types of cell surface receptors such as growth factor receptor and G-protein-coupled receptor. EGFR was highly expressed in pancreatic tissue and has been implicated in PKC activation. Therefore, we investigated the issue of whether a difference exists in the acquisition of the ligand-induced EGFR activation between TGP49-*Fut8*-WT and TGP49-*Fut8*-KDs. As shown in Figure 6A, the core fucosylation on the *N*-glycans of EGFR was diminished in TGP49-*Fut8*-KDs as confirmed by AOL staining. In

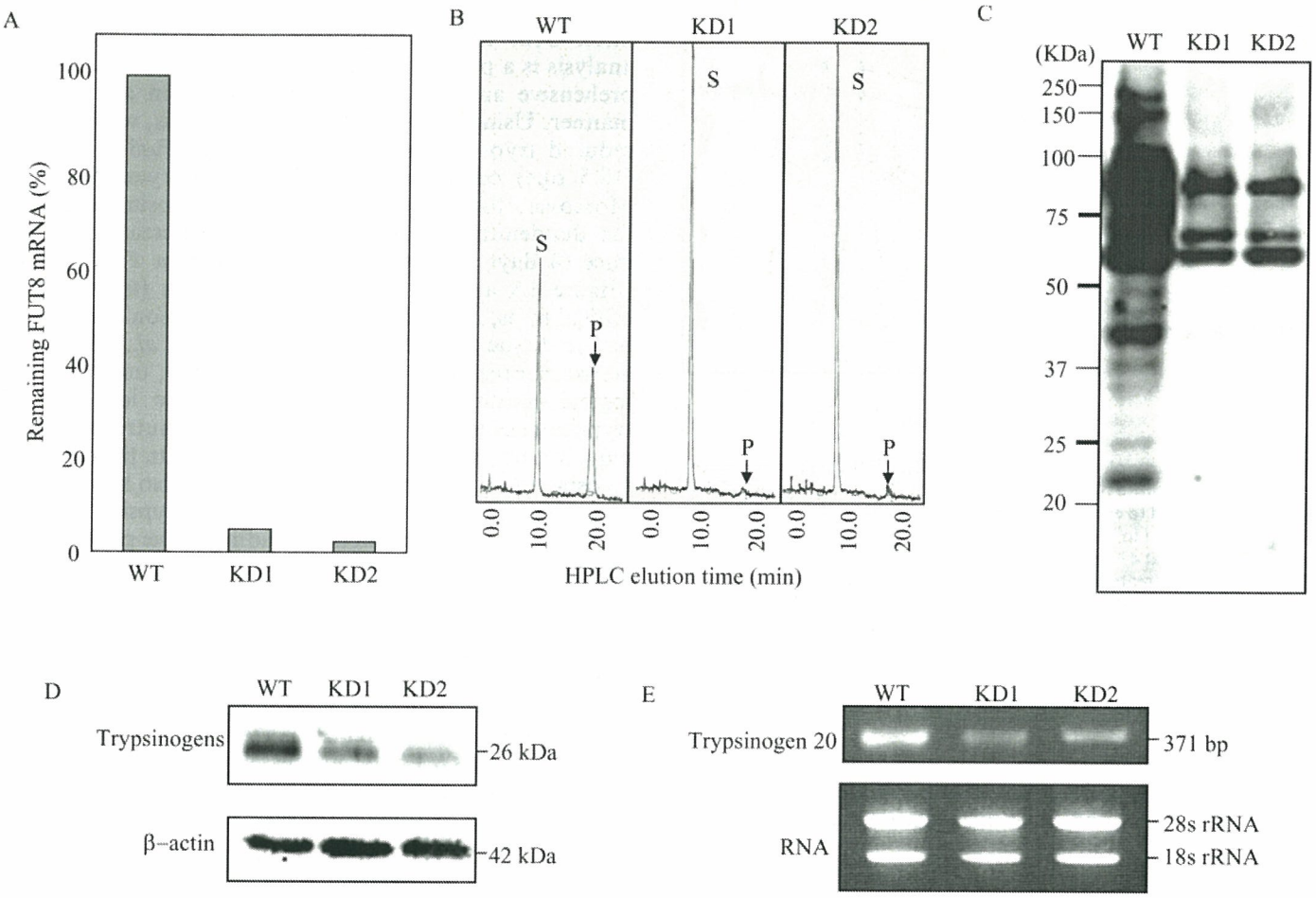


**Fig. 2.** Characterization of TGP49-*Fut8*-KD cells. (**A**) Gene-silencing effects of siRNA on the *Fut8* mRNA expression were determined by real-time PCR and normalized by the levels of GAPDH. (**B**) High-performance liquid chromatography (HPLC) elution profiles of the GnGn-Asn-PABA substrate (S) and the *Fut8* product (P). The large peak at 10 min shows the unreacted substrates, and the peak at 20 min, indicated by an arrow head, is the product. (**C**) Western blots of TGP49-*Fut8*-WT and TGP49-*Fut8*-KDs lysates probed with AAL in 10% gel. The bars indicate the positions of molecular weight markers (Bio-Rad). *Fut8* ablation leads to reduced trypsinogen expression at the mRNA level and the protein level. (**D**) Western blots of TGP49-*Fut8*-WT and TGP49-*Fut8*-KDs cell lysates probed with a rabbit anti-trypsinogen antibody in 12.5% gel. Expression of β-actin is shown as loading control. (**E**) RT–PCR of trypsinogens expression in TGP49-*Fut8*-WT and TGP49-*Fut8*-KDs. The positions of the 28s and 18s rRNAs as well as the sizes of the PCR products are indicated.

contrast to TGP49-*Fut8*-WT, EGF-induced EGFR phosphorylation was attenuated in TGP49-*Fut8*-KD1 without any effect on the total EGFR expression levels at 5 min after stimulation (Figure 6B). The kinetics of receptor phosphorylations was quite similar in both cell lines, reached to the maximal level at 5 min, and returned to the basal level within 30 min. In TGP49-*Fut8*-KD1, the extent of phosphorylation of the receptor was less than half that of TGP49-*Fut8*-WT (Figure 6C). Moreover, we explored the potential role of EGF-associated signaling during the induction of trypsinogen expression by real-time PCR. As anticipated, excess EGF (10 ng/mL) overcame the lower EGFR activity and induced a more than 2-fold higher trypsinogen expression in TGP49-*Fut8*-KD1, which were detectable at 3 and 6 h, as well as TPA (20 nM) stimulation (Figure 7). The c-fos and c-jun are well-known targets of EGF stimulation (Angel and Karin, 1991; Chen and Davis, 2003) and play a variety of roles in many cell functions, such as cell growth and differentiation. In TGP49-*Fut8*-KD1, their mRNA expressions were reduced to about 30% those of TGP49-*Fut8*-WT level. Both EGF (10, 50 ng/mL) and TPA (20, 100 nM) induced several-fold increases in c-fos and c-jun expression, which were detectable at 30 min (Figure 8). EGF-induced c-jun expression in TGP49-derived cells was completely blocked by pretreatment with 1 μM of bisindolylmaleimide (BIM); however, the c-fos expression was partially inhibited, indicating that EGF regulates c-fos and c-jun expression in PKC-dependent and PKC-independent manners (Figure 8). It is noteworthy that EGF-induced trypsinogen expression was preceded by the expression of these two transcription factors, suggesting that c-fos and c-jun are able to directly regulate trypsinogen expression. We also investigated the expression levels of c-fos and c-jun in *Fut8*$^{-/-}$ mice. As expected, the mRNA expression of c-fos and c-jun extracted from the bodies of *Fut8*$^{-/-}$ mice is only 35.4 and 57.4% of *Fut8*$^{+/+}$ mice, respectively (Figure 9). Collectively, these findings therefore suggest that the loss of core fucose residues on *N*-glycans of EGFR attenuated cellular signaling, such as PKC activation, resulting in a reduction in trypsin-PAR-2-regulated growth stimulation.

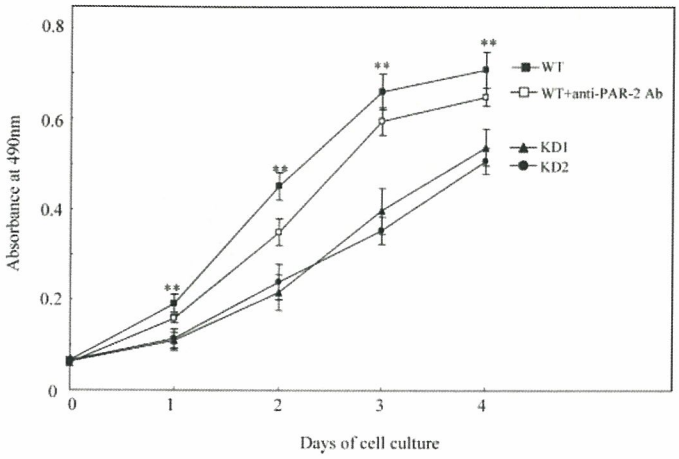


**Fig. 3.** Growth curve of TGP49-derivative cells. All the cells were seeded in a 96-well cell culture plate ($1 \times 10^3$ cells/well). Ten microlitre of CCK-8 solution was added to each well to measure the number of living cells. The absorbances related to the formazan dye level were measured with a microplate reader at 490 nm. Filled square, TGP49-*Fut8*-WT; open square, TGP49-*Fut8*-WT treated by 5 μg/mL of anti-PAR-2 Ab; filled triangle, TGP49-*Fut8*-KD1; and filled circle, TGP49-*Fut8*-KD2. Values are means ± standard deviation (SD) ($N = 3$) of determinations in 1 week. Statistically significant relative to control (**$p < 0.01$).

## Discussion

Because *Fut8* is able to modify multiple proteins and affect their functions, it is necessary to analyze global changes to study the complicated phenotypes of *Fut8*$^{-/-}$ mice. Gene expression profiling using DNA microarray analysis is a powerful and popular approach for the comprehensive analysis of gene expressions in an unbiased manner. Using a DNA microarray analysis, we identified reduced trypsinogen gene expression in *Fut8*$^{-/-}$ embryos (18.5 dpc) compared with *Fut8*$^{+/+}$ embryos (Table I). Moreover, the protein expression of trypsinogens from the duodenum, small intestine, and pancreas in *Fut8*$^{-/-}$ mice (4 days old) was lower than that in *Fut8*$^{+/+}$ mice (Figure 1A and B). Because trypsinogens (trypsin) play critical roles, not only in digestion (Stevenson *et al.*, 1986) but in tissue remodeling (Koshikawa *et al.*, 1998) and acrosomal reactions (Ohmura *et al.*, 1999), under physiological conditions, we speculate that the low level of trypsinogens in *Fut8*$^{-/-}$ mice results in malnutrition, which may, in turn, lead to growth retardation. On the contrary, trypsin, an active form of trypsinogen, is also known to be most potent agonist of the PAR-2. Trypsin activates PAR-2 signaling transduction, leading to the proliferation and differentiation of several types of cells such as epithelial and endothelial cells, fibroblasts, astrocytes, and myocytes (Darmoul *et al.*, 2004; Ossovskaya and Bunnett, 2004). The application of SLIGRL-$NH_2$ (25 μg/mL) rescued the lower growth rates accompanying the down-regulation of trypsinogens, returning them to normal levels in TGP49-*Fut8*-KDs (Figure 5). Moreover, the cell growth of TGP49-*Fut8*-WT was suppressed by the application of an anti-PAR-2 antibody, by up to 60~70% (Figure 3). These findings strongly suggest that reduced PAR-2

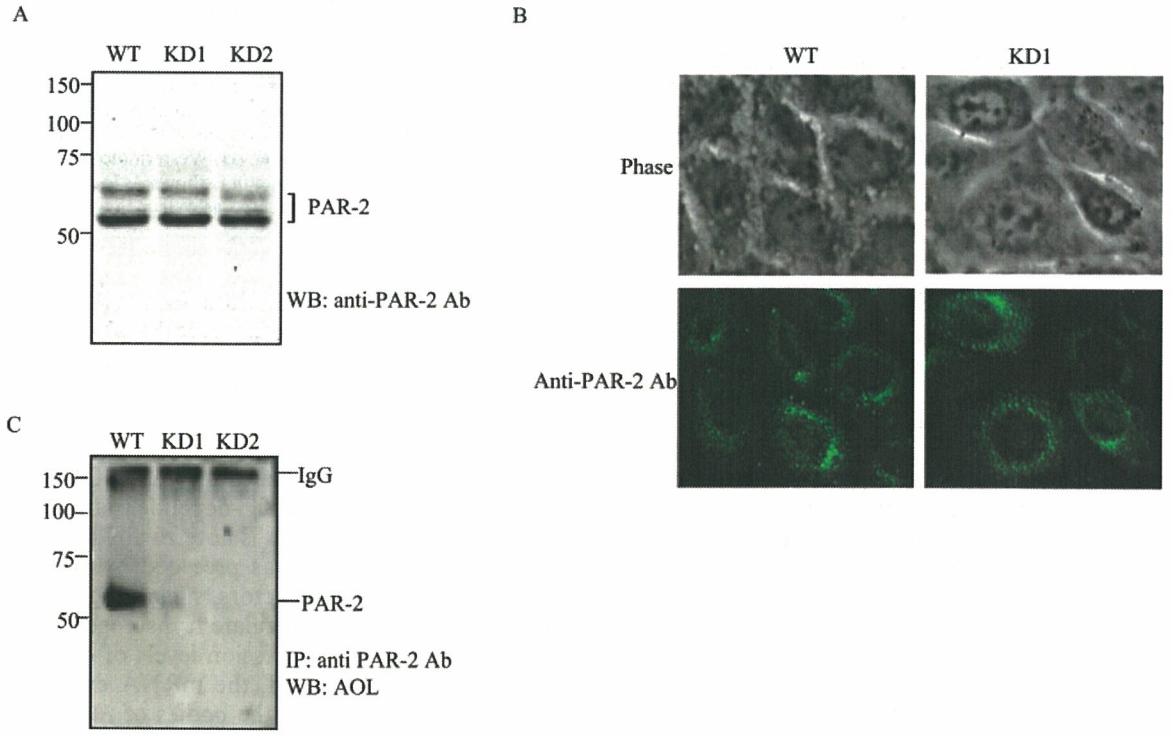


**Fig. 4.** PAR-2 expression levels between TGP49-*Fut8*-WT and TGP49-*Fut8*-KDs. (**A**) Western blot analysis of PAR-2 expression in TGP49-*Fut8*-WT and TGP49-*Fut8*-KDs. (**B**) Abrogation of core fucose of PAR-2 was detected by AOL staining. The immunoprecipitates were treated by Laemmli sample buffer without 2-mercaptoethanol. (**C**) Immunocytochemical staining of TGP49-*Fut8*-WT and TGP49-*Fut8*-KD1 using anti-PAR-2 Ab (green). TGP49-*Fut8*-WT and TGP49-*Fut8*-KD1 cells were grown on glass cover slips for 24 h. Cells were fixed with 4% paraformaldehyde, and indirect immunofluorescence staining was carried out using a monoclonal Ab to PAR-2. Images were acquired using a Leica DMIRB microscope, at a magnification of 200×.

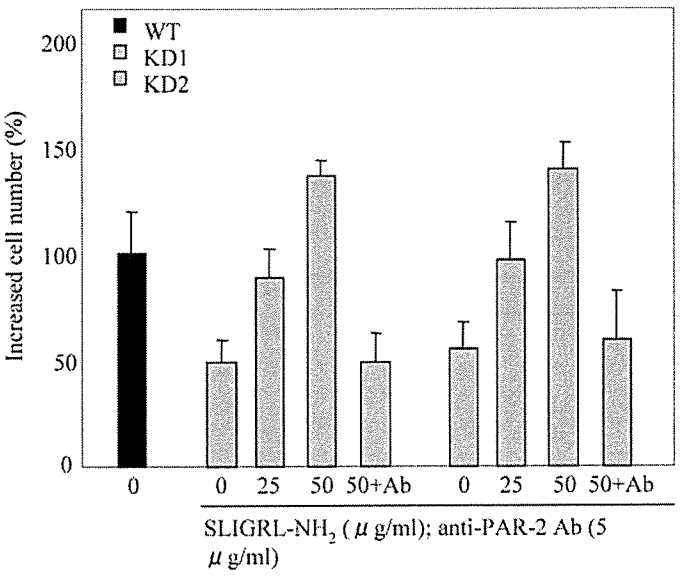


**Fig. 5.** A PAR-2 agonist rescued the growth rates of TGP49-*Fut8*-KDs. Serum-starved cells were treated with SLIGRL-$NH_2$ (at the indicated concentrations). After the treatment, the cells were trypsinized and counted. In addition, the stimulating effects of SLIGRL-$NH_2$ on cell proliferation were significantly inhibited by 5 μg/mL of anti-PAR-2 Ab. Data are reported as the means ± standard deviation (SD) (% of the control) from three replicate cultures.

signaling is directly associated with the slower growth rates seen in TGP49-*Fut8*-KDs.

Trypsinogens are ubiquitously expressed in pancreas, skin, esophagus, stomach, small intestine, large intestine, lung, kidney, liver, bile duck, spleen and brain, and in endothelial and epithelial cells (Koshikawa *et al.*, 1998). In addition to pancreatic trypsin, extrapancreatic trypsin is able to cleave PAR-2 (Alm *et al.*, 2000). PAR-2 is also ubiquitously distributed throughout the entire body of mammals, including the pancreas, kidney, gastrointestinal and respiratory tracts, skin, liver, and heart (Bohm *et al.*, 1996). PAR-2 has been demonstrated to be present in the pancreas and in every region of the gastrointestinal tract and regulates pancreatic and gastric functions. In the pancreas, PAR-2 is expressed by both acinar cells (Bohm *et al.*, 1996; Kawabata *et al.*, 2002) and the duct epithelium (Nguyen *et al.*, 1999), where its activation triggers amylase secretion and electrolyte transport, respectively. Likewise, in the gastrointestinal tract, PAR-2 is expressed at high levels in epithelial cells, and its activation mediates gastrointestinal motility (Corvera *et al.*, 1997) and modulates ion transport (Vergnolle, 2000). Collectively, the widespread distribution of PAR-2 in the pancreas and gastrointestinal tract, coupled with the fact that the pancreas and gastrointestinal tract are exposed to trypsin under physiological conditions, suggests that PAR-2 activation through trypsin is an important modulator in the pancreas and gastrointestinal tract. In *Fut8*$^{-/-}$ mice, we confirmed that trypsinogen (trypsin) expression in the duodenum, small intestine, and pancreas was much lower than that in *Fut8*$^{+/+}$ mice (Figure 1A and B). Thus, reduction of trypsinogen levels resulted in the growth retardation of *Fut8*$^{-/-}$ mice, at least in part, via an attenuation of PAR-2 signaling.

Various studies have reported a role for *N*-glycosylation of EGFR in the direct regulation of receptor functions, including membrane phosphorylation, ligand binding, and signal transduction (Soderquist and Carpenter, 1984). Although specifically how various structures of *N*-glycans modify EGFR function is not known at present, functional studies about EGFR in the overexpressed cells of GnT III, an enzyme that inhibits the extension of *N*-glycans by introducing a bisecting *N*-acetylglucosamine residue, showed that the EGFR displayed a reduced binding affinity for EGF (Rebbaa *et al.*, 1997). Tsuda and others (2000) reported that the removal of *N*-glycans at the $Asn^{420}$ site in EGFR causes a loss of capability to bind EGF, which results in autoactivation of the receptor. The oligosaccharides linked to EGFR have been thoroughly characterized by nuclear magnetic resonance (NMR) and mass spectrometry (Stroop *et al.*, 2000). Over 30 structures have been identified to date, and the major complex-type oligosaccharides contain a di-, tri-, and tetra-antennary structure with core fucosylation. In the present study, we found that core fucose was involved in the phosphorylation of EGFR (Figure 6). In addition, Wang and others (2005, 2006) reported that the binding affinity of TGF-β type II receptor and EGFR toward respective ligands is reduced in mouse embryonic fibroblasts derived from *Fut8*$^{-/-}$ mice, suggesting the involvement of core fucose in ligand binding and the subsequent activation of various receptors. It has been reported that the α1,6-fucosylation could affect the conformation and flexibility of the antenna of *N*-linked bi-antennary oligosaccharides (Stubbs *et al.*, 1996). This might be the case in EGFR conformation. It is conceivable that the lack of core fucose might cause conformational changes in the receptor on the cell surface, subsequently affecting the ligand binding, dimerization, and phosphorylation of the EGFR.

EGFR is coupled to multiple signaling pathways and regulates a wide variety of cellular functions including cell proliferation and differentiation. Mice lacking EGFR show various abnormalities including early death, developmental defects in gastrointestinal organs, etc. (Miettinen *et al.*, 1995). It is important to note that EGFR-deficient mice also show severe defects in the lung, similar to *Fut8*$^{-/-}$ mice (Miettinen *et al.*, 1997). EGF induces c-fos and c-jun via extracellular signal-regulated kinase (ERK)-dependent and PKC-dependent manners in bovine luteal cells (Chen and Davis, 2003). In mammalian cells, ERK and jun N-terminal kinase (JNK) are involved in increasing the amount of c-fos and c-jun, respectively (Karin and Hunter, 1995). The JNK pathway stimulates c-jun activation, which requires the costimulation of both the calcium- and PKC-dependant pathways. Consistent with this, our data indicated that excess EGF induced several-fold increases in c-fos and c-jun expression, and the induced c-jun expression was completely blocked by pretreatment with BIM, but the induced c-fos expression was only partially blocked (Figure 8). Moreover, the level of trypsinogen expression was increased 3 h after the activation of either EGF or TPA. These results suggest that the attenuation of EGF-induced EGFR phosphorylation results in the down-regulation of trypsinogen transcription via the insufficient activation of c-jun and c-fos. It should be noted that the mRNA expression

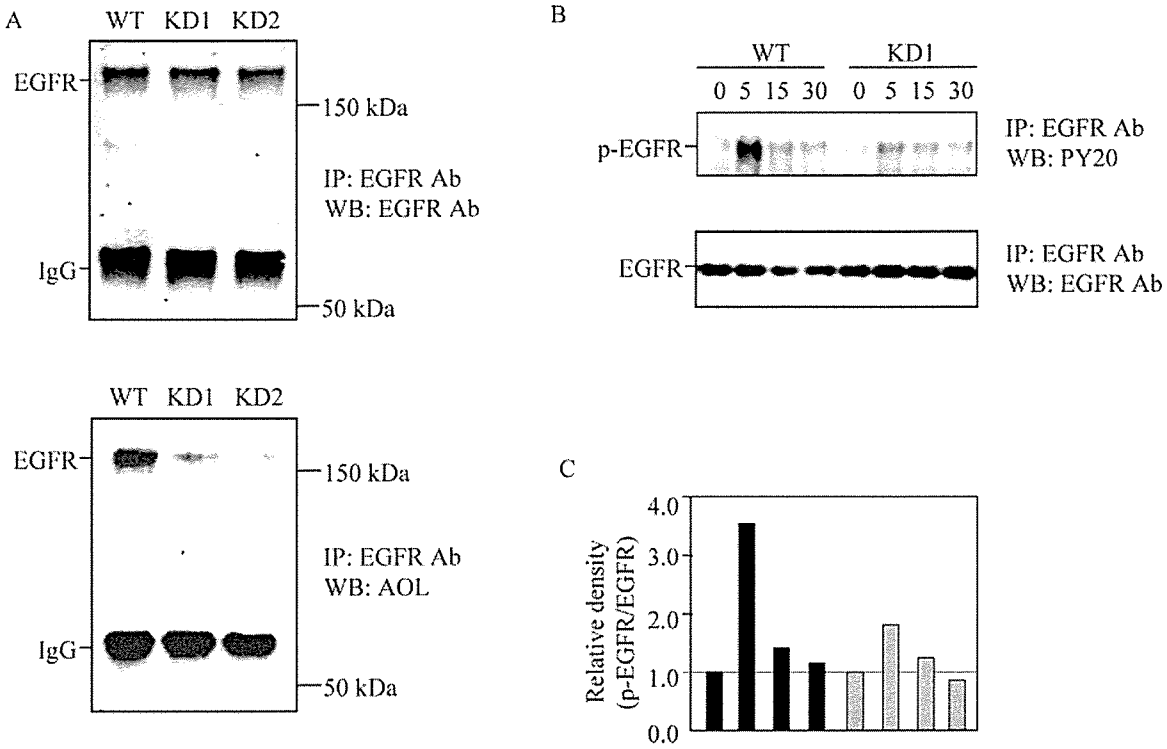


**Fig. 6.** The lack of core fucose on the extracellular domain of EGFR results in desensitization to EGF-induced activation. An antibody to EGFR was used in immunoprecipitation, and the immunoprecipitates were resolved by SDS–PAGE on a 7.5% gel, transferred to a polyvinylidine difluoride (PVDF) membrane and probed with the AOL, anti-EGFR Ab, and PY20. (**A**) Reduction of core fucose of EGFR was detected by AOL staining. The immunoprecipitates were treated with Laemmli sample buffer containing 2-mercaptoethanol. (**B**) Attenuation of phosphorylated forms of EGFR are indicated in western blot. Increased phosphorylation of EGFR was maximal by 5 min. (**C**) Densitometric analysis of the bands of p-EGFR normalized against EGFR.

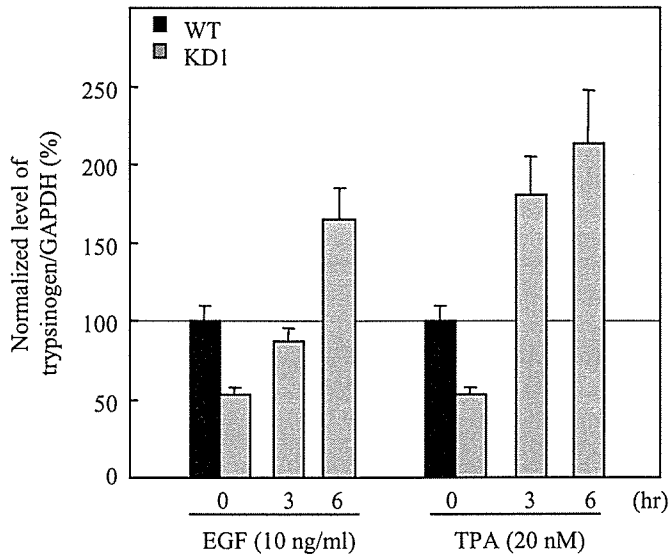


**Fig. 7.** Effects of either EGF or TPA on the expression of trypsinogen mRNAs. Total RNAs were isolated from TGP49-*Fut8*-WT and TGP49-*Fut8*-KD1, and the increase in trypsinogen expression was induced by stimulation with either EGF (10 ng/mL) or TPA (20 nM) at 3 and 6 h. Total RNA (100 ng) were used for the real-time PCR analysis of the trypsinogens mRNA level. GAPDH was used as an internal loading control.

of c-fos and c-jun extracted from the bodies of $Fut8^{-/-}$ mice are only 35.4 and 57.4% that of $Fut8^{+/+}$ mice, respectively (Figure 9), suggesting that the signal transduction initiated by several receptors located on the plasma membrane, like EGFR, might be compromised in $Fut8^{-/-}$ mice.

In summary, the loss of core fucose on the extracellular domain of EGFR affects cell proliferation by modulating EGFR phosphorylation. The low levels of c-fos and c-jun expression in $Fut8^{-/-}$ mice are associated with growth retardation, at least in part, by a reduced trypsinogen expression which, in turn, attenuates the PAR-2-medaited growth signal pathway. The important finding of our study was that core fucose on the extracellular domain of EGFR has an effect on cell proliferation through the regulation of EGFR-trypsin-PAR-2 signaling. Prior studies have shown that tumor-derived trypsin might promote cell proliferation by activation of PAR-2 in several cancers (Miyata *et al.*, 2000; Okamoto *et al.*, 2001; Jin *et al.*, 2003; Ohta *et al.*, 2003; Darmoul *et al.*, 2004). In addition, PAR-2 expression is closely correlated with trypsin expression in tumor tissues (Yamashita *et al.*, 2003). In this regard, our present work provides an attractive opportunity toward a more effective strategy for cancer therapy by de-core fucosylation using the siRNA technique of *Fut8*, as well as the elucidation of the physiological roles of *Fut8*.

## Materials and methods

### *Mice*

Homozygous wild ($Fut8^{+/+}$) and knockout ($Fut8^{-/-}$) mice were obtained by crossing heterozygous $Fut8^{+/-}$ mice. Only

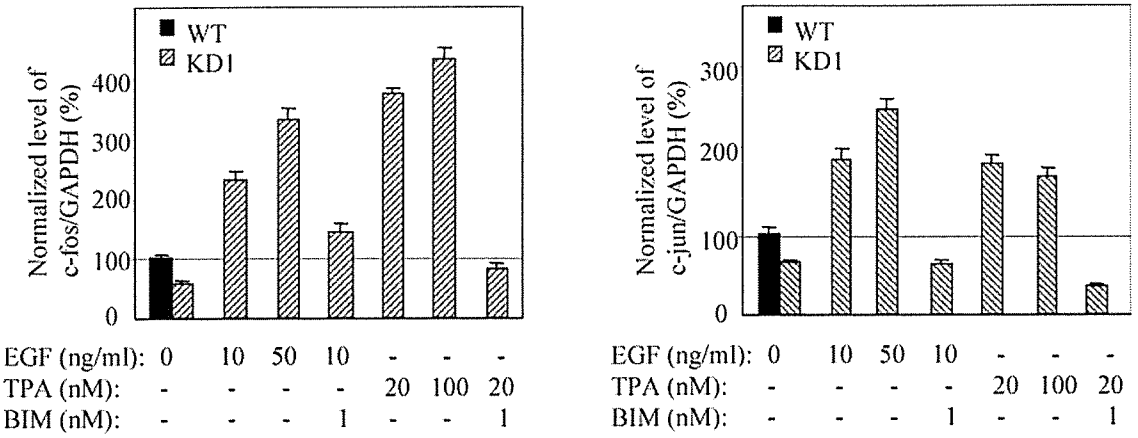


**Fig. 8.** *Fut8* ablation leads to a reduced c-fos and c-jun mRNA expression in TGP49-*Fut8*-KDs, and both EGF and TPA could activate c-fos and c-jun mRNA expression. The low expression of c-fos and c-jun mRNAs in TGP49-*Fut8*-KDs were activated by the application of EGF (10, 50 ng/mL) and TPA (20, 100 nM) for 30 min and blocked by pretreatment with BIM. The PKC inhibitor, BIM, (1 μM) was added to the cells 60 min before the stimuli. Total RNA (100 ng) was used in the real-time PCR analysis of c-fos and c-jun mRNA levels. GAPDH was used as an internal loading control.

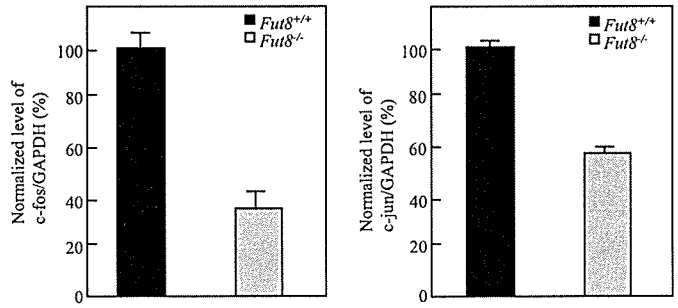


**Fig. 9.** Reduction of c-fos and c-jun mRNA expressions in *Fut8*$^{-/-}$ mice. Expression levels of c-fos and c-jun mRNA (normalized by GAPDH) were determined by real-time PCR. RNA samples were isolated from the bodies both of *Fut8*$^{+/+}$ (18.5 dpc) and of *Fut8*$^{-/-}$ (18.5 dpc) embryos. Total RNA (100 ng) was used for the real-time PCR analysis of the c-fos and c-jun mRNA levels. GAPDH was used as an internal loading control.

male animals of *Fut8*$^{+/+}$ and *Fut8*$^{-/-}$ mice were used in this experiment. Zfy primer: the forward primer 5′-AAGATA AGCTTACATAATCACATGGA-3′ and the reverse primer 5′-CCTATGAAATCCTTTGCTGCACATGT-3′ were used for PCR to distinguish male animals. The mice were maintained in a room illuminated for 12 h (08:00–20:00 h) and kept at 24 ± 1°C with free access to food and water.

### *Antibodies*

The mouse monoclonal anti-PAR-2 $IgG_{2a}$ antibody (sc-13504), mouse monoclonal anti-β-actin $IgG_1$ antibody (sc-8432), rabbit polyclonal anti-uPA antibody (sc-14019), goat polyclonal anti-α1-antitrypsin antibody (sc-14586), and biotin-conjugated anti-goat IgG (sc-2053) were purchased from Santa Cruz (Santa Cruz, CA); anti-rabbit IgG horseradish peroxidase (HRP)-conjugate and anti-mouse IgG HRP-conjugate were from ICN Pharmaceuticals, Inc. (Arora, OH); Alexa Fluor 488-conjugated anti-mouse IgG was from Invitrogen (Carlsbad, CA); anti-phosphotyrosine antibody (PY20) and anti-EGFR antibody were from BD Transduction Laboratories (San Jose, CA). Rabbit polyclonal anti-trypsinogen serum was obtained from Biogenesis (Kingston, NH), and an IgG fraction of the antiserum was purified by affinity chromatography on a HiTrap Protein G HP Columns (Amersham Bioscience, Piscataway, NJ). This antibody was raised against bovine pancreatic trypsinogens. According to the manufacture's protocol, it could cross-react with trypsinogens from various species including mouse and human and several types of trypsinogens.

### *Tissue specimens and sample preparation*

At 18.5 dpc, mother mice were sacrificed by cervical dislocation, and the embryos were quickly removed. *Fut8*$^{+/+}$ and *Fut8*$^{-/-}$ embryonic biopsies were obtained from three mice (one per mouse) for microarray and real-time PCR. Several tissues (pancreas, duodenum, and small intestine) obtained from 4-day-old *Fut8*$^{+/+}$ and *Fut8*$^{-/-}$ mice were immediately fixed in 4% paraformaldehyde for use in immunhistochemical analyses. For protein expression analysis, each tissue was homogenized in 5 volumes (W/V) of ice-cold buffer (50 mM Tris–HCl, 150 mM of NaCl, 1% Triton-100 and 1 mM EGTA) and cleared by centrifugation at 20,000 *g* for 10 min and stored at –80°C until used. The protein concentration of each sample was assayed using a BCA protein assay kit (Pierce, Rockford, IL) according to the manufacturer's protocol.

### *Complementary DNA microarray analysis*

Freshly dissected *Fut8*$^{+/+}$ and *Fut8*$^{-/-}$ embryonic body (18.5 dpc) samples were immediately submerged in 5 volumes of RNAlater (Ambion Inc., Woodward Austin, TX). Total RNA was extracted with TRIzol reagent (Invitrogen), following the protocol recommended by the manufacturer. Approximately 2 μg of total RNA was obtained per mg of embryonic body. Messenger RNA was isolated using a μMACs mRNA Isolation Kit (Miltenyi Biotec., Bergisch Gladbach, Germany). The integrities of total RNA and mRNA were verified by agarose gel electrophoresis and Bioanalyzer with RNA LabChip (Agilent, Palo Alto, CA), following the manufacture's instruction. Messenger RNAs

from three independent experiments were pooled for microarray.

For microarray hybridization, each mRNA (200 ng) was converted to labeled cDNA using RNA Fluorescence Labeling Core Kit (TAKARA Bio. Inc., Shiga, Japan) in the presence of Cy3-dUTP or Cy5-dUTP (Amersham Bioscience), and the labeled cDNA was then purified with Purification Column (TAKARA Bio. Inc.). Each RNA sample was labeled either with Cy3 or with Cy5 for two analyses (i.e., Cy dye swapping). Analysis of gene expression was performed using Takara IntelliGene II Mouse Chip (TAKARA Bio. Inc.), which contains 4285 genes. The hybridizations to the microarray chip were conducted according to the instruction for the Takara DNA Chip Protocol. Fluorescent intensities of the printed cDNA targets were measured using a fluorometric scanning Affymetrix 428 Array Scanner. The microarray images were analyzed using ImaGene v4.1 software. Fold-change levels were calculated, and genes that were regulated with a fold change ≥2 were then selected.

### *Quantitative gene expression analyses by real-time PCR and RT–PCR*

Real-time PCR analyses were performed using a Smart Cycler II System (Cephied, Sunnyvale, CA). The cDNA synthesis was performed using SYBR Green Real-time PCR Core Kit (TAKARA Bio. Inc.) as recommended by manufacturer. Each reaction was performed in a 25 μL volume with final concentration of 1 × SYBR Premix Ex Taq, 200 nM primers, 2 μL of 1:10 dilution of the cDNA and RNase-free water. The thermal cycling conditions for the real-time PCR were 10 s at 95°C to activate SYBR Ex Taq, followed by 40 cycles of denaturation 5 s at 95 °C and annealing/extension for 20 s at 60°C. The mean number of cycles to the threshold of fluorescence detection was calculated for each sample, and glyceraldehyde 3-phosphate dehydrogenase (GAPDH) expression was quantified to normalize the amount of cDNA in each sample. The specificity of the amplified products was monitored by its melting curve.

To determine the effects of EGF and TPA on induction of the expression of c-jun, c-fos, and trypsinogen mRNA, we quantified the amounts of mRNA expression by real-time PCR using SYBR Green Real-time PCR Core Kit (TAKARA Bio. Inc.). Cultures that grew to 80–90% confluence were washed three times with serum-free medium before exposure of either EGF or TPA. In studies involving the pharmacological inhibitor, BIM, the PKC inhibitor, was added to the cells for 60 min before stimuli. After cell stimulation, the cells were rapidly rinsed twice with cold phosphate-buffered saline (PBS), and total RNA was extracted for real-time PCR. The real-time PCR primers are shown in Table II.

Reverse transcription–PCR (RT–PCR) was performed according to the usual method. The primer sequences of trypsinogen 20 were as follows: the forward primer was 5′-TGTTGATTCTGCCAAGATCATC-3′, the reverse primer was 5′-TGCAGCTCTCCATTGCAGACC-3′. Reaction conditions included 94°C for 30 s, 60°C for 1 min, and 72°C for 2 min.

### *Immunohistochemistry*

Immunohistochemical staining was performed on paraformaldehyde-fixed paraffin sections. Briefly, sections were deparaffinized twice in xylene and hydrated through a graded series of ethanol to PBS. Endogenous peroxidase activity was blocked with 3% $H_2O_2$ for 5 min. After washing with PBS containing 0.1% Tween 20 (PBS-T), the slides were blocked with an avidin/biotin blocking kit (Vector Laboratories, Burlingame, CA). The slides were incubated with either anti-trypsinogen IgG or biotin-conjugated AOL (Ishida *et al.*, 2002) and washed three times with PBS-T. After washing, the antibody-incubated slide was treated with biotin-conjugated anti-rabbit IgG for 1 h. The slides were washed again and then covered with HRP-streptavidin (Vector Laboratories) for 30 min. Finally, the slides were visualized with 3, 3′-diaminobenzidine and counterstained with hematoxylin and eosin.

### *Measurement of FUT8 activity*

The specific activity of FUT8 was determined as described previously (Uozumi *et al.*, 1996). Briefly, a 5-μg sample as the enzyme source was mixed with the assay buffer (200 mM MES [pH 7.0], 1% Triton X-100, 500 μM donor [GDP-L-fucose], 50 μM acceptor [GnGn-Asn-4-(2-pyridylamine) butylamine {PABA}]). After incubation at 37°C, the reaction was stopped by boiling. Ten microliters of the supernatant was subjected to high-performance liquid chromatography (HPLC) with a Fluorescent detector (Ex. 310 nm and Em. 380 nm). Activity was expressed as pmol of GDP-fucose transferred to the acceptor per hour per milligram of protein.

### *Cells culture*

The pancreatic acinar cell carcinoma TGP49, in which trypsinogen is expressed (Pettengill *et al.*, 1994), was obtained from ATCC (Manassas, VA; CRL-2136) and maintained in DMEM:Ham's F12 (1:1) medium (Sigma, St. Louis, MO) supplemented with 10% heat-inactivated fetal bovine serum (FBS), 2 mM Glutamine, 50 units/mL of penicillin, and 50 μg/mL of streptomycin (Sigma, St. Louis, MO). The medium was changed every 3 days. The subculture was conducted by washing the cells with PBS and adding 0.25% trypsin/1 mM ethylenediaminetetraacetic acid (EDTA) (Nakalai tesque, Kyoto, Japan) for 5 min. Trypsinized cells were counted, centrifuged, and resuspended in fresh medium. Cell lysates were prepared by scraping cells with ice-cold buffer (50 mM Tris–HCl, 150 mM of NaCl, 1% Triton-X 100, and 1 mM EGTA), followed by sonication. The lysate was cleared by centrifugation at 20,000 × *g* for 10 min at 4 °C.

### *Transient transfection of Fut8 siRNA*

TGP49 cells ($5 \times 10^4$) were seeded in six-well plates and allowed to grow to 90% confluence. Transient transfections of *Fut8* siRNAs were performed with *TransIT*-TKO transfection reagent (TAKARA Bio. Inc.) according to the manufacturer's instructions. The siRNAs were designed to form 19-bp dsRNA with 2 thymine overhangs at both 3′ ends. Four targeting sequences of the *Fut8* siRNA used are as follows: No.2 (sense: 5′-UGGAGCUAAAGAGCUCUGGTT-3′, antisense:

3′-TTACCUCGAUUUCUCGAGACC-5′); No 5 (sense: 5′-CAGCUUGUUAAGGCCAAAGTT-3′, antisense: 3′-TTGUCGAACAAUUCCGGUUUC-5′); No 8 (sense: 5′-CAGGCUUAUAUCCCUCCUATT-3′, antisense: 3′-TTGUCCGAAUAUAGGGAGGAU-5′); and No 16 (sense: 5′-UCUCAGAAUUGGCGCUAUGTT-3′, antisense: 3′-TTAGAGUCUUAACCGCGAUAC-5′). Alexa 488-conjugated siRNA duplex (Qiagen, Hilden, Germany) was used to define the transfection efficiency.

*Establishment of Fut8 knockdown cell lines*

A retrovirusvecor carrying siRNA targeted to *Fut8* (No.16) was constructed as follows. A 21-nucleotide sequence of the *Fut8* gene was inserted in the sense and antisense directions into the pSINsi-mU6 cassette vector (recombinant retrovirus vector) (TAKARA Bio. Inc.) containing the mouse U6 promoter. The recombinant retroviruses were generated by co-transfection of the vector mixture such as recombinant retrovirus vector, pE-eco vector (ecotropic *env*), and pGP vector (*gag-pol*) to HEK293 cells. Recombinant retrovirus particles containing the target sequence or a mock control were infected into the parental TGP49 cells, and the geneticin (G418)-resistant clones were selected as a stable tranfectant. The TGP49 derivative cell lines stably transfected with the plasmid-expressing siRNA that targeted FUT8 are referred to hereafter as "GP49-*Fut8*-KD"and with the empty plasmid as "GP49-*Fut8*-WT."

*Cell growth assay*

The growth rate of cells was measured using the Cell Counting Kit-8 (CCK-8) (Wako, Osaka, Japan). Each cell line was grown in 96-well tissue culture dishes at 37°C in DMEM:Ham's F12 (1:1) medium containing 10% FBS and 200 μg/mLof G418. Ten microliters of CCK-8 solution to each well was used for measuring the number of living cells. The absorbance related to the formazan dye level was measured with a microplate reader (Corona Electric Co., Ibaraki, Japan) at 490 nm. To determine the proliferative effect of the PAR-2 agonists in the TGP 49 cell culture, the cells were treated with or without activating peptide SLIGRL-$NH_2$ (25 and 50 μg/mL) (Sigma) in DMEM:Ham's F12 (1:1) medium containing 2% bovine serum albumin (BSA). After an appropriate period of incubation, the rate of cell growth was assessed with a hemacytometer.

*Fluorescence immunocytochemistry and confocal microscopy*

For cellular localization of PAR-2 in TGP49 cells, each cell line was seeded on a FALCON and BIOCOAT culture slide (four chambers; Becton Dickinson Labware, Meylan Cedex, France). When the cells reached subconfluence, they were washed with PBS (PBS+: 0.9 mM $CaCl_2$ and 0.5 mM $MgCl_2$) and fixed with 4% paraformaldehyde. After washing with PBS, cells were blocked with 5% BSA in PBS+. Following a PBS rinse, they were incubated with the PAR-2 antibody (1:20) for 1 h at room temperature. Following incubation with the secondary antibody (1:300) conjugated with Alexa Fluor 488, the cells were washed and mounted in anti-fade medium (PermaFluor Mamtant Medium; Immunon, Pittsburgh, PA). The slides were examined under a fluorescence microscope (Leica, Cambridge, UK) at a 200× magnification using the appreciate filter.

*Western blot and lectin blot analysis*

The protein samples were electrophoresed on 12.5% polyacrylamide gels using Mini Protean II electrophoresis tanks (Bio-Rad, Hercules, CA). After electrophoresis, proteins were transferred to polyvinylidine difluoride (PVDF) membranes (Immobilon-P, 0.45 μm, Millipore, Bedford, MA,) at 240 mA for 60 min. Blots were blocked for 2 h with 5% skim milk in TBS-T (10 mM Tris–HCl, pH 7.5, 150 mM NaCl, and 0.1% Tween 20) or with 5% BSA in TBS-T. Following incubation with the appropriate primary antibodies or fucose lectin overnight, the slides were washed. After washing, the blots were incubated with the corresponding secondary antibodies conjugated with HRP or ABC reagent (Vector Laboratories). Finally, specific proteins were visualized using an ECL system (Amersham Pharmacia Biotech AB, Uppsala, Sweden). The fucose lectins used were AOL and AAL (Yazawa *et al.*, 1984), both of which preferentially recognize core fucosylation on *N*-glycans.

*Phosphorylation status of EGFR*

Serum starvation of TGP49 cells was accomplished by substitution of 2% (w/v) BSA for 10% FBS in the culture medium before the experiments. Stimulations were carried out at 37°C in 25 mM Tris–HCl (pH 7.4) including 120 mM NaCl, 5 mM KCl, 1.2 mM $MgCl_2$, and 2% (w/v) BSA. Serum-starved cells were treated with EGF (1 nM) for 0, 5, 15, and 30 min. Stimulations were terminated by washing the cells once with ice-cold PBS supplemented with 0.4 mM sodium orthovanadate and then harvested by scraping. Cells were collected and solubilized for 15 min at 4°C in lysis buffer (50 mM Tris–HCl [pH 8.0], 1% [v/v] Triton X-100, 150 mM NaCl, 10% [v/v] glycerol, 2 mM EDTA, 100 μM phenylmethylsulfonylfluoride, 5 μg/mL of leupeptin, 1 of μg/mL aprotinin, 100 mM NaF, and 1 mM sodium orthovanadate). After lysis, the lysate was centrifuged at 20,000 *g* for 10 min at 4 °C to precipitate insoluble materials, and the detergent extracts (supernatant) were subjected to immunoprecipitation or directly electrophoresed and immunoblotted, as indicated below.

*Immunoprecipitation*

For immunoprecipitation, cell extracts (500~1000 μg) were mixed with 20 μL of a 50% suspension of Protein G-Sepharose (Amersham Pharmacia Biotech AB) and incubated at 4°C for 2 h with continuous rotation. Ten microliters of polyclonal anti-EGFR Ab or anti-PAR-2 IgG was added and incubated at 4°C overnight with gentle agitation. The beads were washed four times with lysis buffer. The immunoprecipitated samples were eluted from the protein G-Sepharose by heating at 100°C for 5 min in Laemmli sample buffer with or without 2-mercaptoethanol. After centrifugation, the supernatants were resolved by SDS–PAGE and western blotted.

*Statistical analysis*

The results are expressed as mean value ± standard deviation (SD). Statistical analyses were carried out using Student's *t*-test. A *p*-value <0.05 was considered statistically significant.

## Supplementary data

Supplementary data are available at Glycobiology online (http://glycob.oxfordjournals.org/). Fig. 1: Real-time PCR analysis of various glycosyltransferases in TGP49 derived cells. Fig. 2: uPA expressions in cell culture media of TGP49 derived cells. Concentrated cell culture supernatants of TGP49-derivative cells were run on 10% gel and probed with a rabbit anti-uPA polyclonal antibody. CBB staining is shown as a loading control.

## Acknowledgments

We thank Dr Ihara of Osaka University for the GnGn-Asn-PABA acceptor. We also thank Dr Milton S. Feather for editing the manuscript. This work was supported by a CREST and the 21st Century COE Program from the Ministry of Education, Science, Culture, Sports, and Technology of Japan. Funding to pay the Open Access publication charges for this article was provided by the authors.

## Conflict of interest statement

None declared.

## Abbreviations

AAL, *Aleuria aurantia* lectin; AOL, *Aspergillus oryzae* lectin; BIM, bisindolylmaleimide; BSA, bovine serum albumin; dpc, days postcoitum; CCK-8, Cell Counting Kit-8; EDTA, ethylenediaminetetraacetic acid; EGFR, epidermal growth factor receptor; FBS, fetal bovine serum; Fut8, α1,6-fucosyltransferase; GAPDH, glyceraldehyde 3-phosphate dehydrogenase; GnT III, *N*-acetylglucosaminyltransferase III; HRP, horseradish peroxidase; Ig, immunoglobulin; PAR-2, proteinase-activated receptor 2; PCR, polymerase chain reaction; PBS, phosphate-buffered saline; PKC, protein kinase C; PVDF, polyvinylidine difluoride; siRNA, short interfering RNA; RT–PCR, reverse transcription–polymerase chain reaction; TGF-β, transforming growth factor-β; TPA, 12-*O*-tetradecanoylphorbol-13-acetate; uPA, urokinase-type plasminogen activator; β4GalT-I, β1,4-galactosyltransferase I.

## References

Alm, A.K., Gagnemo-Persson, R., Sorsa, T., and Sundelin, J. (2000) Extrapancreatic trypsin-2 cleaves proteinase-activated receptor-2. *Biochem. Biophys. Res. Commun.*, **275**, 77–83.

Angel, P. and Karin, M. (1991) The role of Jun, Fos and the AP-1 complex in cell-proliferation and transformation. *Biochim. Biophys. Acta.*, **1072**, 129–157.

Bohm, S.K., Kong, W., Bromme, D., Smeekens, S.P., Anderson, D.C., Connolly, A., Kahn, M., Nelken, N.A., Coughlin, S.R., Payan, D.G., and Bunnett, N.W. (1996) Molecular cloning, expression and potential functions of the human proteinase-activated receptor-2. *Biochem. J.*, **314** (Pt 3), 1009–1016.

Carpenter, G. and Cohen, S. (1990) Epidermal growth factor. *J. Biol. Chem.*, **265**, 7709–7712.

Chen, D.B., and Davis, J.S. (2003) Epidermal growth factor induces c-fos and c-jun mRNA via Raf-1/MEK1/ERK-dependent and -independent pathways in bovine luteal cells. *Mol. Cell Endocrinol.*, **200**, 141–154.

Corvera, C.U., Dery, O., McConalogue, K., Bohm, S.K., Khitin, L.M., Caughey, G.H., Payan, D.G., and Bunnett, N.W. (1997) Mast cell tryptase regulates rat colonic myocytes through proteinase-activated receptor, 2. *J. Clin. Invest.* **100**, 1383–1393.

Damiano, B.P., Cheung, W.M., Santulli, R.J., Fung-Leung, W.P., Ngo, K, Ye, R.D., Darrow, A.L., Derian, C.K., de Garavilla, L., and Andrade-Gordon, P. (1999) Cardiovascular responses mediated by protease-activated receptor-2 (PAR-2) and thrombin receptor (PAR-1) are distinguished in mice deficient in PAR-2 or PAR-1. *J. Pharmacol. Exp. Ther.*, **288**, 671–678.

Darmoul, D., Gratio, V., Devaud, H., and Laburthe, M. (2004) Protease-activated receptor 2 in colon cancer: trypsin-induced MAPK phosphorylation and cell proliferation are mediated by epidermal growth factor receptor transactivation. *J. Biol. Chem.* **279**, 20927–20934.

Domino, S.E., Zhang, L., Gillespie, P.J., Saunders, T.L., and Lowe, J.B. (2001) Deficiency of reproductive tract alpha(1,2)fucosylated glycans and normal fertility in mice with targeted deletions of the FUT1 or FUT2 alpha(1,2)fucosyltransferase locus. *Mol. Cell Biol.*, 21, 8336–8345.

Elbashir, S.M., Harborth, J., Lendeckel, W., Yalcin, A., Weber, K., and Tuschl, T. (2001) Duplexes of 21-nucleotide RNAs mediate RNA interference in cultured mammalian cells. *Nature*, **411**, 494–498.

Guo, P., Wang, Q.Y., Guo, H.B., Shen, Z.H., and Chen, H.L. (2004) N-acetylglucosaminyltransferase V modifies the signaling pathway of epidermal growth factor receptor. *Cell Mol. Life. Sci.*, **61**, 1795–1804.

Homeister, J.W., Thall, A.D., Petryniak, B., Maly, P., Rogers, C.E., Smith, P.L., Kelly, R.J., Gersten, K.M., Askari, S.W., Cheng, G., and others. (2001) The alpha(1,3)fucosyltransferases FucT-IV and FucT-VII exert collaborative control over selectin-dependent leukocyte recruitment and lymphocyte homing. *Immunity*, **15**, 115–126.

Ishida, H., Moritani, T., Hata, Y., Kawato, A., Suginami, K., Abe, Y., and Imayasu, S. (2002) Molecular cloning and overexpression of fleA gene encoding a fucose-specific lectin of Aspergillus oryzae. *Biosci. Biotechnol. Biochem.*, **66**, 1002–1008.

Jin, E., Fujiwara, M., Pan, X., Ghazizadeh, M., Arai, S., Ohaki, Y., Kajiwara, K., Takemura, T., and Kawanami, O. (2003) Protease-activated receptor (PAR)-1 and PAR-2 participate in the cell growth of alveolar capillary endothelium in primary lung adenocarcinomas. *Cancer*, **97**, 703–713.

Kahn, M.L., Hammes, S.R., Botka, C., and Coughlin, S.R. (1998) Gene and locus structure and chromosomal localization of the protease-activated receptor gene family. *J. Biol. Chem.*, **273**, 23290–23296.

Karin, M. and Hunter, T. (1995) Transcriptional control by protein phosphorylation: signal transmission from the cell surface to the nucleus. *Curr. Biol.*, **5**, 747–757.

Kawabata, A., Kuroda, R., Nishida, M., Nagata, N., Sakaguchi, Y., Kawao, N., Nishikawa, H., Arizono, N., and Kawai, K. (2002) Protease-activated receptor-2 (PAR-2) in the pancreas and parotid gland: immunolocalization and involvement of nitric oxide in the evoked amylase secretion. *Life Sci.*, **71**, 2435–2446.

Koshikawa, N., Hasegawa, S., Nagashima, Y., Mitsuhashi, K., Tsubota, Y., Miyata, S., Miyagi, Y., Yasumitsu, H., and Miyazaki, K. (1998) Expression of trypsin by epithelial cells of various tissues, leukocytes, and neurons in human and mouse. *Am. J. Pathol.*, **153**, 937–944.

Koshikawa, N., Nagashima, Y., Miyagi, Y., Mizushima, H., Yanoma, S., Yasumitsu, H., and Miyazaki, K. (1997) Expression of trypsin in vascular endothelial cells. *FEBS Lett.*, **409**, 442–448.

Kudo, T., Kaneko, M., Iwasaki, H., Togayachi, A., Nishihara, S., Abe, K., and Narimatsu, H. (2004) Normal embryonic and germ cell development in mice lacking alpha 1,3-fucosyltransferase IX (Fut9) which show disappearance of stage-specific embryonic antigen 1. *Mol Cell Biol.* **24**, 4221–4228.

Maly, P., Thall, A., Petryniak, B., Rogers, C.E., Smith, P.L., Marks, R.M., Kelly, R.J., Gersten, K.M., Cheng, G., Saunders, T.L., and others (1996) The alpha(1,3)fucosyltransferase Fuc-TVII controls leukocyte trafficking through an essential role in L-, E-, and P-selectin ligand biosynthesis. *Cell*, **86**, 643–653.

Miettinen, P.J., Berger, J.E., Meneses, J., Phung, Y., Pedersen, R.A., Werb, Z., and Derynck, R. (1995) Epithelial immaturity and multiorgan

failure in mice lacking epidermal growth factor receptor. *Nature*, **376**, 337–341.

Miettinen, P.J., Warburton, D., Bu, D., Zhao, J.S., Berger, J.E., Minoo, P., Koivisto, T., Allen, L., Dobbs, L., Werb, Z., and others. (1997) Impaired lung branching morphogenesis in the absence of functional EGF receptor. *Dev. Biol.*, **186**, 224–236.

Miyata, S., Koshikawa, N., Yasumitsu, H., and Miyazaki, K. (2000) Trypsin stimulates integrin alpha(5)beta(1)-dependent adhesion to fibronectin and proliferation of human gastric carcinoma cells through activation of proteinase-activated receptor-2. *J. Biol. Chem.*, **275**, 4592–4598.

Nguyen, T.D., Moody, M.W., Steinhoff, M., Okolo, C., Koh, D.S., and Bunnett, N.W. (1999) Trypsin activates pancreatic duct epithelial cell ion channels through proteinase-activated receptor-2. *J. Clin. Invest.*, **103**, 261–269.

Nystedt, S., Emilsson, K., Wahlestedt, C., and Sundelin, J. (1994) Molecular cloning of a potential proteinase activated receptor. *Proc. Natl Acad. Sci. U. S. A.*, **91**, 9208–9212.

Ohmura, K., Kohno, N., Kobayashi, Y., Yamagata, K., Sato, S., Kashiwabara, S., and Baba, T. (1999) A homologue of pancreatic trypsin is localized in the acrosome of mammalian sperm and is released during acrosome reaction. *J. Biol. Chem.*, **274**, 29426–29432.

Ohta, T., Shimizu, K., Yi, S., Takamura, H., Amaya, K., Kitagawa, H., Kayahara, M., Ninomiya, I., Fushida, S., Fujimura, T., and others (2003) Protease-activated receptor-2 expression and the role of trypsin in cell proliferation in human pancreatic cancers. *Int. J. Oncol.*, **23**, 61–66.

Okamoto, T., Nishibori, M., Sawada, K., Iwagaki, H., Nakaya, N., Jikuhara, A., Tanaka, N., and Saeki, K. (2001) The effects of stimulating protease-activated receptor-1 and -2 in A172 human glioblastoma. *J. Neural. Transm.* **108**, 125–140.

Ossovskaya, V.S. and Bunnett, N.W. (2004) Protease-activated receptors: contribution to physiology and disease. *Physiol. Rev.*, **84**, 579–621.

Pettengill, O.S., Memoli, V.A., Brinck-Johnsen, T., and Longnecker, D.S. (1994) Cell lines derived from pancreatic tumors of Tg(Ela-1-SV40E)Bri18 transgenic mice express somatostatin and T antigen. *Carcinogenesis*, **15**, 61–65.

Pratt, R.M., and Pastan, I. (1978) Decreased binding of epidermal growth factor to BALB/c 3T3 mutant cells defective in glycoprotein synthesis. *Nature*, 272, 68–70.

Rebbaa, A., Yamamoto, H., Saito, T., Meuillet, E., Kim, P., Kersey, D.S., Bremer, E.G., Taniguchi, N., and Moskal, J.R. (1997) Gene transfection-mediated overexpression of beta1,4-N-acetylglucosamine bisecting oligosaccharides in glioma cell line U373 MG inhibits epidermal growth factor receptor function. *J. Biol. Chem.*, **272**, 9275–9279.

Schena, M., Shalon, D., Davis, R.W., and Brown, P.O. (1995) Quantitative monitoring of gene expression patterns with a complementary DNA microarray. *Science*, **270**, 467–470.

Shimamoto, R., Sawada, T., Uchima, Y., Inoue, M., Kimura, K., Yamashita, Y., Yamada, N., Nishihara, T., Ohira, M., and Hirakawa, K. (2004) A role for protease-activated receptor-2 in pancreatic cancer cell proliferation. *Int. J. Oncol.*, **24**, 1401–1406.

Smith, P.L., Myers, J.T., Rogers, C.E., Zhou, L., Petryniak, B., Becker, D.J., Homeister, J.W., and Lowe, J.B. (2002) Conditional control of selectin ligand expression and global fucosylation events in mice with a targeted mutation at the FX locus. *J. Cell Biol.*, **158**, 801–815.

Soderquist, A.M. and Carpenter, G. (1984) Glycosylation of the epidermal growth factor receptor in A-431 cells. The contribution of carbohydrate to receptor function. *J. Biol. Chem.*, **259**, 12586–12594.

Stevenson, B.J., Hagenbuchle, O., and Wellauer, P.K. (1986) Sequence organisation and transcriptional regulation of the mouse elastase II and trypsin genes. *Nucleic Acids Res.*, **14**, 8307–8330.

Stroop, C.J., Weber, W., Gerwig, G.J., Nimtz, M., Kamerling, J.P., and Vliegenthart, J.F. (2000) Characterization of the carbohydrate chains of the secreted form of the human epidermal growth factor receptor. *Glycobiology*, **10**, 901–917.

Stubbs, H.J., Lih, J.J., Gustafson, T.L., and Rice, K.G. (1996) Influence of core fucosylation on the flexibility of a biantennary N-linked oligosaccharide. *Biochemistry*, **35**, 937–947.

Tsuda, T., Ikeda, Y., and Taniguchi, N. (2000) The Asn-420-linked sugar chain in human epidermal growth factor receptor suppresses ligand-independent spontaneous oligomerization. Possible role of a specific sugar chain in controllable receptor activation. *J. Biol. Chem.*, **275**, 21988–21994.

Uchima, Y., Sawada, T., Nishihara, T., Umekawa, T., Ohira, M., Ishikawa, T., Nishino, H., and Hirakawa, K. (2003) Identification of a trypsinogen activity stimulating factor produced by pancreatic cancer cells: its role in tumor invasion and metastasis. *Int. J. Mol. Med.*, **12**, 871–878.

Uozumi, N., Teshima, T., Yamamoto, T., Nishikawa, A., Gao, Y.E., Miyoshi, E., Gao, C.X., Noda, K., Islam, K.N., Ihara, Y., and others (1996) A fluorescent assay method for GDP-L-Fuc:N-acetyl-beta-D-glucosaminide alpha 1–6fucosyltransferase activity, involving high performance liquid chromatography. *J. Biochem. (Tokyo)* **120**, 385–392.

Vergnolle, N. (2000) Review article: proteinase-activated receptors – novel signals for gastrointestinal pathophysiology. *Aliment Pharmacol. Ther.*, **14**, 257–266.

Wang, X., Gu, J., Yamamoto, T., Nishikawa, A., Gao, Y.E., Miyoshi, E., Gao, C.X., Noda, K., Islam, K.N., Ihara, Y., and others (2006) Core fucosylation regulates epidermal growth factor receptor-mediated intracellular signaling. *J. Biol. Chem.*, **281**, 2572–2577.

Wang, X., Inoue, S., Wang, X., Inoue, S., Gu, J., Miyoshi, E., Noda, K., Li, W., Mizuno-Horikawa, Y., Nakano, M., and others (2005) Dysregulation of TGF-{beta}1 receptor activation leads to abnormal lung development and emphysema-like phenotype in core fucose-deficient mice. *Proc. Natl Acad. Sci. U. S. A.*, **102**, 15791–15796.

Wilson, J.R., Williams, D., and Schachter, H. (1976) The control of glycoprotein synthesis: N-acetylglucosamine linkage to a mannose residue as a signal for the attachment of L-fucose to the asparagine-linked N-acetylglucosamine residue of glycopeptide from alpha1-acid glycoprotein. *Biochem. Biophys. Res. Commun.*, **72**, 909–916.

Yamashita, K., Mimori, K., Inoue, H., Mori, M., and Sidransky, D. (2003) A tumor-suppressive role for trypsin in human cancer progression. *Cancer Res.*, **63**, 6575–6578.

Yazawa, S., Furukawa, K., and Kochibe, N. (1984) Isolation of fucosyl glycoproteins from human erythrocyte membranes by affinity chromatography using Aleuria aurantia lectin. *J. Biochem. (Tokyo)*, **96**, 1737–1742.

Supplemental Material can be found at:
http://www.jbc.org/cgi/content/full/M605697200/DC1

THE JOURNAL OF BIOLOGICAL CHEMISTRY VOL. 281, NO. 40, pp. 29797–29806, October 6, 2006
© 2006 by The American Society for Biochemistry and Molecular Biology, Inc. Printed in the U.S.A.

# Fucosylation of *N*-Glycans Regulates the Secretion of Hepatic Glycoproteins into Bile Ducts*[S]

Received for publication, June 14, 2006 Published, JBC Papers in Press, August 9, 2006, DOI 10.1074/jbc.M605697200

**Tsutomu Nakagawa[‡], Naofumi Uozumi[‖], Miyako Nakano[‡], Yoko Mizuno-Horikawa[‡], Noriko Okuyama[‡], Tomohiko Taguchi[‡], Jianguo Gu[‡], Akihiro Kondo[§], Naoyuki Taniguchi[¶], and Eiji Miyoshi[‡‖1]**

*From the Departments of [‡]Biochemistry, and [§]Glycotherapeutics, Osaka University Graduate School of Medicine, the [¶]Department of Disease Glycomics, Research Institute for Microbial Diseases, Osaka University, 565-0871 Osaka, Japan and [‖]Japan Science and Technology Agency, 4-1-8 Honcho Kawaguchi, 332-0012 Saitama, Japan*

**Fucosylated α-fetoprotein (AFP) is a highly specific tumor marker for hepatocellular carcinoma (HCC). However, the molecular mechanism by which serum level of fucosylated AFP increases in patients with HCC remains largely unknown. Here, we report that the fucosylation of glycoproteins could be a possible signal for secretion into bile ducts in the liver. We compared oligosaccharide structures on glycoproteins in human bile with those in serum by several types of lectin blot analyses. Enhanced binding of biliary glycoproteins to lectins that recognize a fucose residue was observed over a wide range of molecular weights compared with serum glycoproteins. A structural analysis of oligosaccharides by two-dimensional mapping high performance liquid chromatography and matrix-assisted laser desorption ionization time-of flight mass spectrometry confirmed the increases in the fucosylation of biliary glycoproteins. Purification followed by structural analysis on α1-antitrypsin, α1-acid glycoprotein and haptoglobin, which are synthesized in the liver, showed higher fucosylation in bile than in serum. To find direct evidence for fucosylation and sorting signal into bile ducts, we used α1–6 fucosyltransferase (Fut8)-deficient mice because fucosylation of glycoproteins produced in mouse liver was mainly an α1–6 linkage. Interestingly, the levels of α1-antitrypsin and α1-acid glycoprotein were quite low in bile of Fut8-deficient mice as compared with wild-type mice. An immunohistochemical study showed dramatic changes in the localization of these glycoproteins in the liver of Fut8-deficient mice. Taken together, these results suggest that fucosylation is a possible signal for the secretion of glycoproteins into bile ducts in the liver. A disruption in this system might involve an increase in fucosylated AFP in the serum of patients with HCC.**

Fucosylated α-fetoprotein (AFP)[2], referred to as the L3 band of AFP on LCA (Lensculinaris agglutinin) lectin affino electrophoresis, is a highly specific tumor marker for hepatocellular carcinoma (HCC). Increases in AFP levels in serum are observed in patients with chronic liver disease such as liver cirrhosis, but fucosylated AFP is barely detectable in benign liver diseases (1). α1–6 fucosyltransferase (Fut8) is involved in fucosylation of AFP, and we previously succeeded in the purification and cDNA cloning of Fut8 from porcine brain (2) and a human gastric cancer cell line (3). Although the overexpression of Fut8 in Hep3B cells increased the fucosylation rate of AFP, a high expression of Fut8 was also observed in non-cancerous liver cirrhotic tissues as well as HCC tissues (4). Therefore, other factors could be linked to specific incidences of fucosylated AFP in HCC. GDP-fucose is a donor substrate for Fut8. Recently, we developed an assay system for GDP-fucose levels in cells/tissues (5). When we determined GDP-fucose levels in liver tissues using the assay system, the levels in HCC tissues were significantly higher than those in liver cirrhosis and normal liver (6). The increases of GDP-fucose in HCC were due to the enhancement of FX (human homologue of GDP-4-keto-6-deoxymannose-3,5-epimerase-4-reductase) expression, which contributed to the synthesis of GDP-fucose. Therefore, both Fut8 and FX would regulate the production of fucosylated AFP in HCC. However, increases in Fut8 and FX in HCC tissues were two or three times compared with their surrounding tissues, and another factor could be concerned in terms of increases in fucosylated AFP in serum of patients with HCC.

The sorting of glycoproteins to apical or basolateral membranes in polarized cells is a recent hot spot for discussions in cell biology. An apical sorting machinery is hardly known although polarized cells such as Madin-Darby canine kidney cells have been widely used to investigate the sorting mechanism. In experiments using Madin-Darby canine kidney cells, *N*-glycans are considered possible candidates of apical sorting signal based on the findings that some proteins gain

* This work was supported in part by Grants-in-aid for Scientific Research (S) (13854010) and (C) (16590245), the Special Coordination Funds for Promoting Science and Technology, and the 21st Century Center of Excellence Program from the Ministry of Education, Culture, Sports, Science, and Technology of Japan. A part of this work was supported by Japan Science and Technology Agency and the New Energy and Industrial Technology Development Organization as part of a research and development project related to medical glycology. The costs of publication of this article were defrayed in part by the payment of page charges. This article must therefore be hereby marked "*advertisement*" in accordance with 18 U.S.C. Section 1734 solely to indicate this fact.

[S] The on-line version of this article (available at http://www.jbc.org) contains supplemental Fig. S1.

[1] To whom correspondence should be addressed: Dept. of Biochemistry, Osaka University Graduate School of Medicine, 2-2 Yamada-oka, Suita, 565-0871 Osaka, Japan. Tel.: 81-6-6879-3421; Fax: 81-6-6879-3429; E-mail: miyoshi34@biochem.med.osaka-u.ac.jp.

[2] The abbreviations used are: AFP, α-fetoprotein; HCC, hepatocellular carcinoma; Fut8, α1–6 fucosyltransferase; AAT, α1-antitrypsin; HPLC, high performance liquid chromatography; MALDI-TOF MS, matrix-assisted laser desorption ionization time-of flight mass spectrometry; AAL, *Aleuria aurantia*; SSA, *Sambucus sieboldiana*; MAM, *Maackia amurensis*; ConA, *Canavalia ensiformis*; AOL, *Aspergillus oryzae*; Hp, haptoglobin; AGP, α1-acid glycoprotein; TBS, Tris-buffered saline; PA, pyridylamino.

Downloaded from www.jbc.org at OSAKA UNIVERSITY on April 8, 2007

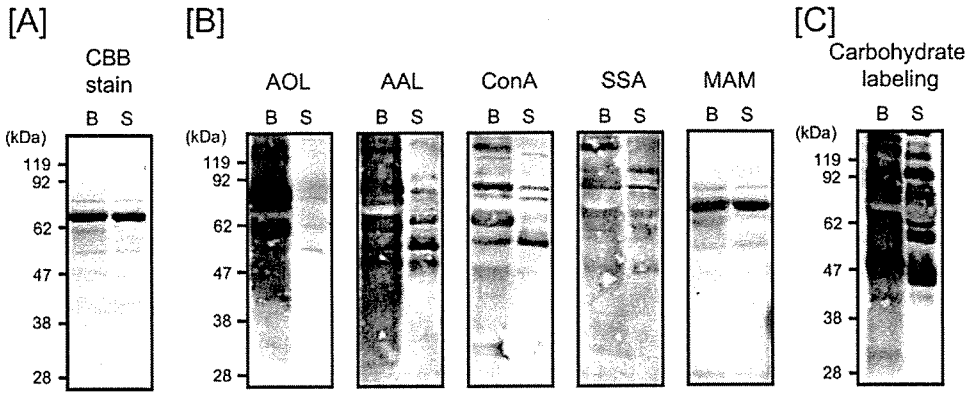


FIGURE 1. **Comparison of human biliary and serum glycoproteins.** 5 μg of proteins from human bile and serum were subjected to 12% SDS-PAGE and stained with Coomassie Brilliant Blue (*A*). Lectin blot analyses were performed using the same samples (*B*). AOL and AAL bind to fucose residue. ConA binds with high affinity to a high mannose-type, biantennary complex or hybrid type of asparagine-linked oligosaccharide. SSA and MAM bind to α2–6- and α2–3-linked sialic acid residues, respectively. 5 μg of protein from human bile and serum were subjected to 12% SDS-PAGE, and glycosylated proteins were detected according to the manufacturer's protocol for the ECL glycoprotein detection system (Amersham Biosciences) (*C*). *B* and *S* indicate bile and serum, respectively. Detailed procedures are described under "Experimental Procedures."

the ability to reach the apical membrane after the recombinant addition of an *N*-glycosylation site and that other proteins entirely or partially lose apical expression as a result of the removal of *N*-glycans by amino acid mutation or treatment with glycosylation inhibitors (7–11). It was also reported that the core region sugars, not sialic acid and galactose, were more important than the terminal sugars for apical sorting (12, 13).

In the case of the liver, major epithelial cells, hepatocytes, produce a variety of serum glycoproteins and non-glycosylated proteins, including albumin. In the system of hepatocytes, there are two kinds of secretion pathways. One pathway is to an apical surface of hepatocytes followed by secretion into bile ducts. The other is to the basolateral surface followed by secretion into blood vessels. Interestingly, the same kinds of serum proteins, including albumin, are detected in bile (14). Until now, however, few cellular or protein factors have been found to regulate these secretion pathways.

In serum glycoproteins, both α1-antitrypsin (AAT) and transferrin were reported to be fucosylated in patients with HCC (15). However, because these two glycoproteins are produced in normal hepatocytes, the rate of fucosylation of these glycoproteins that could occur in HCC tissues was quite low. The expression of Fut8 is enhanced in cirrhotic hepatocytes, leading to a slight increase in fucosylated glycoproteins in these cells even though the levels of GDP-fucose are not higher compared with HCC tissues (6). Where are these fucosylated glycoproteins produced by cirrhotic hepatocytes? To answer this question, we hypothesized that the fucosylation of glycoproteins might be a signal for sorting to the bile ducts. This hypothesis leads to the selective secretion of fucosylated glycoproteins into bile ducts. In the present study, we analyzed oligosaccharide structures on biliary glycoproteins compared with those on serum glycoproteins. Many biliary glycoproteins were strongly fucosylated compared with those in the serum as evidenced by lectin blot analyses as well as high performance liquid chromatography (HPLC) and matrix-assisted laser desorption ionization time-of flight mass spectrometry (MALDI-TOF MS) analyses. Furthermore, we found that the sorting system of hepatic glycoproteins is disrupted in Fut8-deficient mice.

## EXPERIMENTAL PROCEDURES

*Materials*—Biotinated lectins (AAL (*Aleuria aurantia*), ConA (*Canavalia ensiformis*), SSA (*Sambucus sieboldiana*), and MAM (*Maackia amurensis*)) were purchased from Seikagaku Corp. (Tokyo, Japan). Biotinated AOL (*Aspergillus oryzae*) and AOL-agarose were from Toyo Kasei Kogyo Co., Ltd. (Tokyo, Japan). Both AAL and AOL bind to fucose residues with the α1–2, 1–3, 1–4, and 1–6 linkage. ConA binds with high affinity to a high mannose-type, biantennary complex or hybrid type of asparagine-linked oligosaccharide. SSA and MAM bind to α2–6- and α2–3-linked sialic acid residues, respectively.

*Animals*—8-week-old BALB/c mice were used. The establishment of Fut8-deficient mice has been described previously (16). Body weight, liver weight/body weight, serum protein concentration, and bile protein concentration for wild-type and Fut8-deficient mice were 24.9 ± 0.57 g, 6.22 ± 0.31, 49.5 ± 3.6 mg/ml, 3.69 ± 0.42 mg/ml and 15.4 ± 1.51 g, 5.05 ± 0.28, 49.3 ± 1.8 mg/ml, 4.45 ± 2.17 mg/ml (mean ± S.D., $n = 3$), respectively. Although a ratio of liver weight/body weight of Fut8-deficient mice was significantly smaller than that of wild-type mice, no significant differences between the two types of mice were observed in serum and bile protein concentrations. There was no difference in the volume of bile secretion between the two types of mice. All procedures of animal experiments were performed in accordance with the Animal Ethics Committee of Osaka University.

*Bile Specimens*—Human bile was collected from a percutaneous transcatheter drainage tube in a patient with obstructive jaundice due to common bile duct stones. This collection was performed according to an ethical committee of Osaka University Hospital. Serum was collected from the same patient. Mice were anesthetized with ketamine and xylazine (0.8 mg and 0.08 mg/10 g body weight, respectively). Bile duct cannulation was carried out according to the method of Fischer *et al.* (17). Shortly, the abdomen was opened, and the gallbladder was ligated with a string. The common bile duct was cannulated with a 30-gauge needle connected to polyethylene tubing. Gallbladder bile was collected after the extraction. Protein concentrations of bile specimens were measured with a bicinchoninic acid protein assay kit (Pierce, Rockford, IL) using bovine serum albumin as a standard after delipidation according to the method of Wessel and Flugge (18).

*Purification of Human AAT, Haptoglobin (Hp), and α1-Acid Glycoprotein (AGP) from Serum and Bile*—Human AAT, Hp, and AGP were purified from serum by a separate two-step

Downloaded from www.jbc.org at OSAKA UNIVERSITY on April 8, 2007

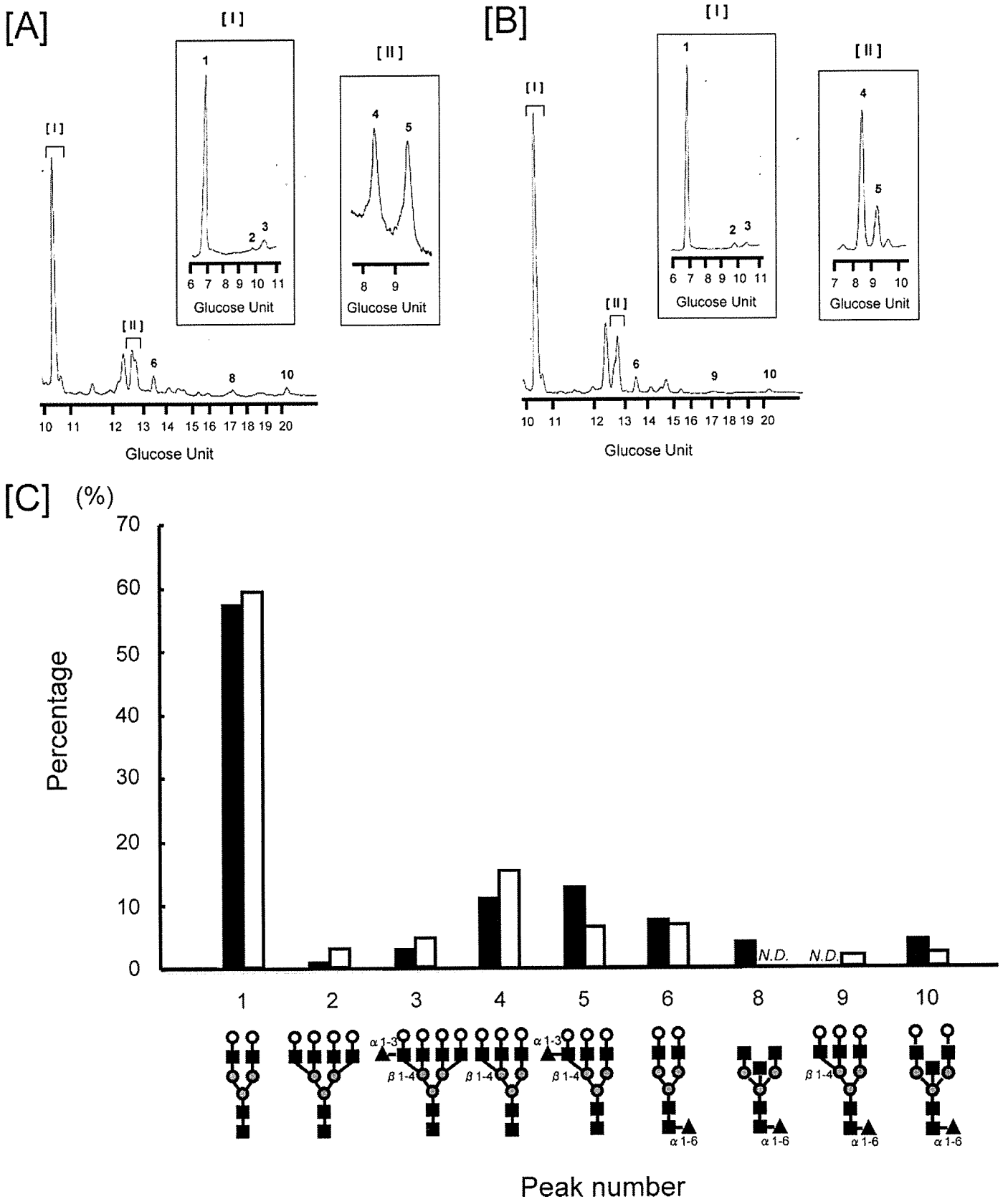


FIGURE 2. **HPLC separation of PA oligosaccharides from human biliary and serum glycoproteins.** Representative elution profile of PA oligosaccharides from human bile (*A*) and serum (*B*) on an ODS column. The charts in *frames* indicate an elution profile on an Amido-80 column of peak (*I*) or (*II*) on an ODS column. Detailed procedures are described under "Experimental Procedures." The percentages of each peak in the total area of assigned peaks were calculated based on peak areas of ODS and Amide-80 elution profiles (*C*). *Numbers* at each peak correspond to those in Table 1. *Closed* and *open columns* indicate oligosaccharides from biliary and serum glycoproteins, respectively. *N.D.*, not detected.

Downloaded from www.jbc.org at OSAKA UNIVERSITY on April 8, 2007

**TABLE 1**
**Assignment of the major PA oligosaccharides by two-dimensional mapping HPLC and MALDI-TOF MS analyses**

| Peak[a] | Structure[b] | ODS[c] (GU) | Amide-80[c] (GU) | m/z |
|---|---|---|---|---|
| 1 | | 10.3 | 6.9 | 1719.7[d] |
| 2 | | 10.3 | 9.9 | 2450.1[d] |
| 3 | β 1-4, α 1-3 | 10.3 | 10.6 | 2597.6[d] |
| 4 | β 1-4 | 12.8 | 8.4 | 2107.3[e] |
| 5 | β 1-4, α 1-3 | 12.8 | 9.1 | 2254.0[e] |
| 6 | α 1-6 | 13.5 | 7.3 | 1888.4[e] |
| 7 | α 1-6 | 13.5 | 10.3 | 2597.6[d] |
| 8 | α 1-6 | 17.0 | 5.9 | 1744.8[d] |
| 9 | α 1-6, β 1-4 | 17.0 | 8.6 | 2254.0[e] |
| 10 | α 1-6 | 20.3 | 7.3 | 2068.9[d] |

[a] Numbers at each peak indicated correspond to those in Figs. 2, 4, and 6.
[b] Monosaccharides were denoted by ○, galactose; ■, *N*-acetylglucosamine; ◎, mannose; △, fucose.
[c] The elution positions on HPLC columns were expressed as glucose units (GU). The chromatographic conditions were described under "Experimental Procedures."
[d] The ions correspond to $[M + H]^+$.
[e] The ions correspond to $[M + Na]^+$.

chromatography procedure. In the first step, albumin was removed from the serum by chromatography on an Econo-Pac Blue Cartridge (Bio-Rad Laboratories) using 20 mM sodium phosphate buffer, pH 7.1. The protein eluate from an Econo-Pac Blue Cartridge was concentrated on an Apollo concentrator (Orbital Sciences Corp., Topsfield, MA) and then re-equilibrated in 50 mM sodium phosphate buffer, pH 7.4, containing 0.5 M NaCl on a PD-10 column (Amersham Biosciences). The re-equilibrated eluate was then used directly in chromatography on antibody columns equilibrated with the same buffer. In the second chromatographic step on antibody columns, the re-equilibrated eluate was recirculated a fifth time. After washing with equilibration buffer, the elution of bound fraction was performed by 0.1 M glycine-HCl, pH 3.0.

To purify glycoproteins from human bile, bile was equilibrated in 50 mM sodium phosphate buffer, pH 7.4, containing



Downloaded from www.jbc.org at OSAKA UNIVERSITY on April 8, 2007

0.5 M NaCl on PD-10 columns. These bile samples were then used directly in chromatography on antibody columns. The same methods as with serum were performed.

*Lectin Blot Analysis*—Lectin blot analyses were performed as described previously (19). Briefly, 5–10 μg of proteins were subjected to 12% SDS-PAGE. After the electrophoresis, the gels were blotted onto nitrocellulose membranes. The membranes were incubated with 3% bovine serum albumin in Tris-buffered saline (20 mM Tris, 0.5 M NaCl, pH 7.5; TBS) overnight and then incubated with 1.0 μg/ml of biotinated lectins (AOL, AAL, ConA, SSA, MAM) in TBST (TBS containing 0.05% Tween 20) for 1 h. After washing with TBST, the membranes were incubated with horseradish peroxidase-conjugated avidin (VECTASTAIN ABC kit; Vector Laboratories, Burlingame, CA) for 1 h and then washed with TBST. Staining was performed with ECL Western blot detection reagents (Amersham Biosciences).

*Fractionation of Human Biliary and Serum AGP by AOL Lectin Affinity Chromatography*—AOL lectin affinity chromatography was performed at room temperature, using AOL-agarose column (bed volume 2 ml) and equilibrated with 10 mM Tris, 0.5 M NaCl, pH 7.4. AGP purified from human bile and serum were equilibrated in the same buffer on PD-10 column and were concentrated using an Apollo concentrator. Purified AGP sample was applied to the column. The elution of non-bound fraction was performed by five volumes of equilibration buffer, and each fraction of 0.5 ml was collected. The elution of bound fraction was performed using 50 mM fucose in equilibration buffer. Protein concentrations were assayed by spectrophotometry at 280 nm.

*Western Blot Analysis*—5–10 μg of proteins were subjected to 12% SDS-PAGE. After the electrophoresis, the gels were blotted onto nitrocellulose membranes. The membranes were incubated with 2% skim milk in TBS for 1 h and then incubated with 1/1000 diluted rabbit anti-human AAT, Hp (Dako Cytomation, Copenhagen, Denmark), goat anti-human AAT (Santa Cruz Biotechnology, Santa Cruz, CA), rabbit anti-mouse AGP (Life Diagnostics, Inc., West Chester, PA), 10 μg/ml of rabbit anti-human AGP (Abcam Ltd., Cambridgeshire, UK), and horseradish peroxidase-conjugated goat anti-mouse albumin (Bethyl Laboratories, Inc., Montgomery, TX) antibodies in 2% skim milk in TBST overnight for human AAT, Hp, mouse AAT, AGP, human AGP, and mouse albumin, respectively. The membranes, except for mouse albumin, were incubated with 1/1000 diluted HRP-conjugated anti-rabbit IgG (Promega, Madison, WI) or anti-goat IgG (Dako Cytomation) antibody in 2% skim milk in TBST for 1 h after washing with TBST three times for 10 min each. Staining was performed with ECL Western blot detection reagents after washing with TBST three times for 10 min each.

*Structural Analysis of Oligosaccharides from Biliary and Serum Glycoproteins*—Bile and serum were equilibrated in 20 mM sodium phosphate buffer, pH 7.1, on PD-10 columns. Immunoglobulins were removed by using Protein A-Sepharose (Sigma) and Protein G-Sepharose 4 Fast Flow (Amersham Biosciences). The solutions were subjected to trichloroacetic acid precipitation, and the precipitated fraction was washed with ethanol twice. Oligosaccharides were released from the precipitated proteins and AAT, Hp, and AGP purified from bile and serum by hydrazinolysis (100 °C for 10 h) followed by *N*-acetylation (20).

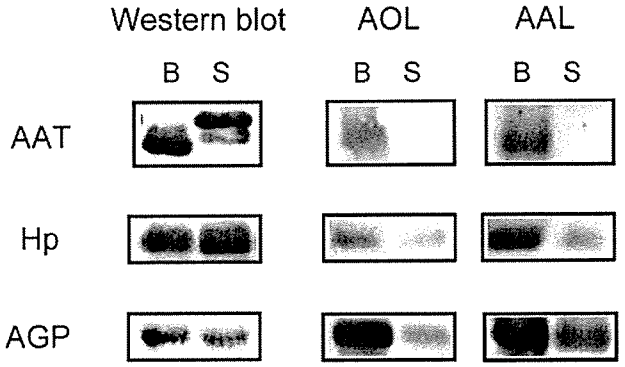


FIGURE 3. **Lectin blot analyses of AAT, Hp,and AGP purified from human bile and serum.** AAT, Hp, and AGP purified from human bile and serum were subjected to 12% SDS-PAGE, and Western blot and lectin blot analyses were performed. AOL and AAL bind to fucose residue. *B* and *S* indicate bile and serum, respectively. Detailed procedures are described under "Experimental Procedures."

The oligosaccharides were applied to the GlycoTAG (Takara Bio Inc., Shiga, Japan) for pyridylamination (21). Excess reagents were removed by chromatography on a TSK gel Amide-80 column (Tosoh Corp., Tokyo, Japan). Sialic acids of the purified pyridylamino (PA) oligosaccharides were removed with neuraminidase treatment (from *Arthrobacter ureafaciens*, Nacalai Tesq, Kyoto, Japan) in 0.2 M acetate buffer, pH 7.4, at 37 °C overnight. The asialo PA oligosaccharides were separated by reverse phase HPLC on a Shim-pack CLC-ODS column (Shimadzu Corp., Kyoto, Japan) and subsequent normal phase HPLC on a TSK gel Amide-80 column. Elution and detection of PA oligosaccharides were performed as described by Tomiya *et al.* (22). The structures of PA oligosaccharides were determined from the elution position of each peak in combination with α-fucosidase (from bovine kidney; Sigma) and β-galactosidase (from *Aspergillus oryzae*; Sigma) digestion.

*MALDI-TOF MS*—MALDI-TOF MS of PA oligosaccharides was performed on an Ultraflex TOF/TOF mass spectrometer equipped with a reflector and controlled by the Flexcontrol 1.2 software package (Bruker Daltonics GmbsH, Bremen, Germany). In MALDI-TOF MS reflector mode using positive polarity, ions generated by a pulsed UV laser beam (nitrogen laser, l = 337 nm, 5 Hz) were accelerated to a kinetic energy of 15 kV. A solution of 2,5-dihydroxybenzoic acid (Bruker Daltonics) in a mixture of ethanol-0.1% trifluoroacetic acid (1:2) (10 mg/ml) was used as matrix. Sample (1 μl) was added to the matrix solution (4 μl), and a part of the mixture (1 μl) was then applied to a polished stainless steel target (Bruker Daltonics).

*Immunohistochemical Analysis*—To detect the AAT and AGP in the mouse liver using immunohistochemical technique, whole liver tissues from wild-type or Fut8-deficient mice were fixed by 0.1 M phosphate buffer containing 4% paraformaldehyde and embedded in paraffin. For immunohistochemical analysis, the dewaxed sections were pretreated with hydroxygen blocking and nonspecific staining reagent (Dako Cytomation) for 10 min at 37 °C and then incubated with 1/200 diluted goat anti-human AAT antibody (Santa Cruz Biotechnology) and 1/300 diluted rabbit anti-mouse AGP antibody (Life Diag-

Downloaded from www.jbc.org at OSAKA UNIVERSITY on April 8, 2007

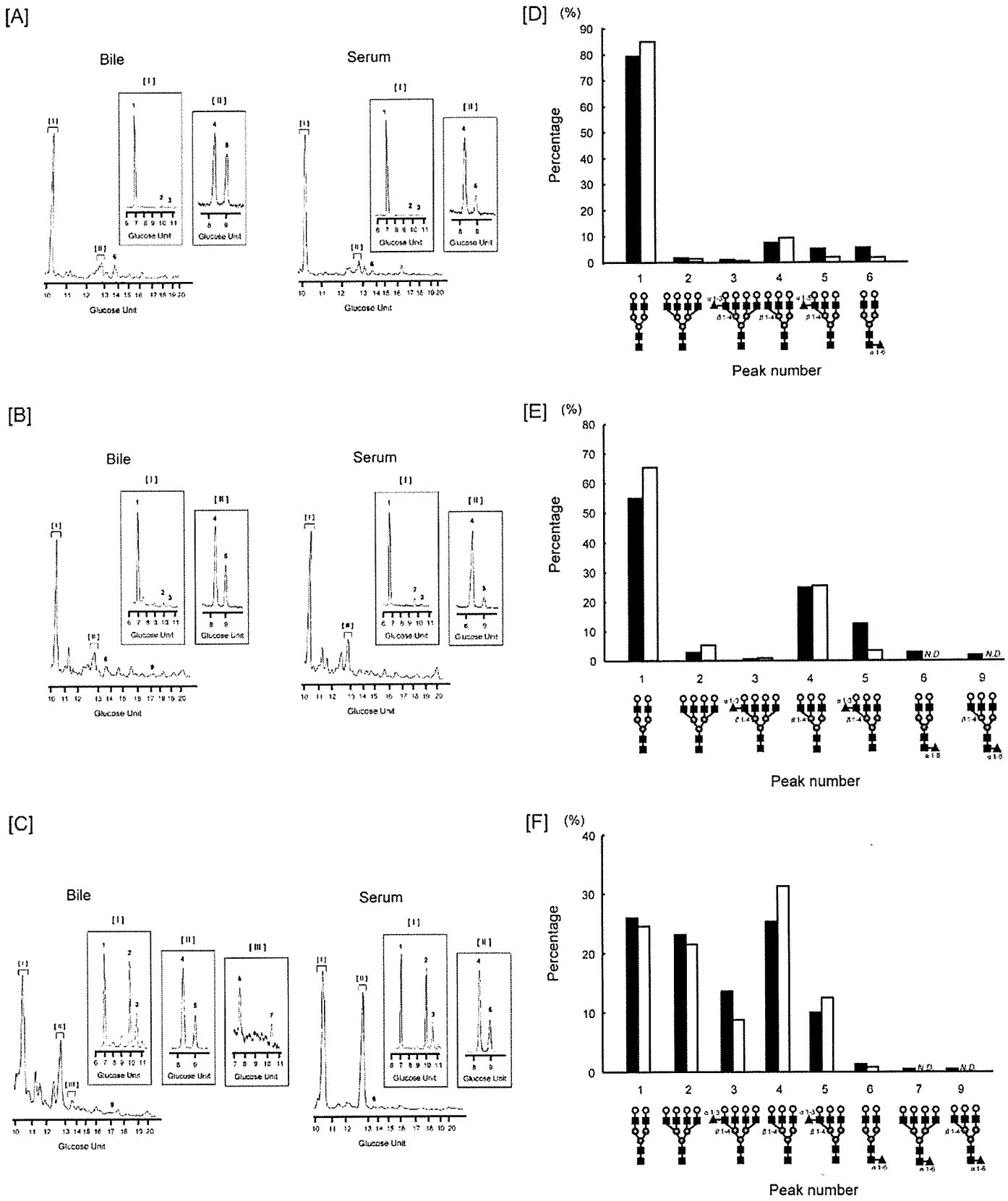


FIGURE 4. **HPLC separations of PA oligosaccharides from AAT, Hp, and AGP purifed from human bile and serum.** Representative elution profile of PA oligosaccharides from AAT (*A*), Hp (*B*), and AGP (*C*) purified from human bile and serum on an ODS column. The charts in *frames* indicate the elution profile on an Amido-80 column for peaks (*I-III*) on an ODS column. Detailed procedures are described under "Experimental Procedures." The percentages of each peak in the total area of assigned peaks were calculated based on peak areas of ODS and Amide-80 elution profiles (*D*, AAT; *E*, Hp; *F*, AGP). *Numbers* at each peak correspond to those in Table 1. *Closed* and *open columns* indicate oligosaccharides from glycoproteins purified from bile and serum, respectively. *N.D.*, not detected.

Downloaded from www.jbc.org at OSAKA UNIVERSITY on April 8, 2007

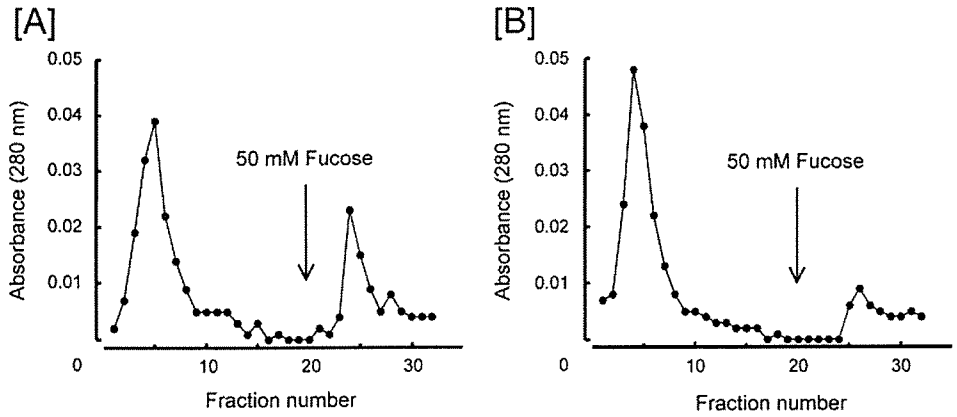


FIGURE 5. **Fractionation of human biliary and serum AGP by AOL lectin affinity chromatography.** AGP purified from human bile (*A*) and serum (*B*) was applied to the AOL-agarose colomn (bed volume 2 ml) equilibrated with 10 mM Tris, 0.5 M NaCl, pH 7.4, at room temperature. Fractions of 0.5 ml were collected, and their respective absorbance (280 nm) was measured. After five volumes of equilibration buffer were applied to elute non-bound fraction, 50 mM fucose was introduced (indicated by an *arrow*) to the elute-bound fraction.

nostics) in antibody diluent buffer (Dako Cytomation) at 4 °C overnight and at room temperature for 1 h for AAT and AGP, respectively. The sections were followed by a second reaction with 1/200 diluted horseradish peroxidase-conjugated anti-goat IgG and anti-rabbit IgG antibodies (Dako Cytomation) for AAT and AGP, respectively.

The immunoreactivity was visualized using the manufacturer's protocol for the peroxidase/3, 3′-diaminobenzidine tetrahydrochloride reagent in the DAB kit (Dako Cytomation), and sections were counterstained with Gills' hematoxylin solution. The immunostainings were photographed using a microscope system (Microphot F-XA; Nikkon, Tokyo, Japan) and application (Photograb-250; Fuji Film, Tokyo, Japan).

## RESULTS

*The Comparison of Oligosaccharide Structures between Human Biliary and Serum Glycoproteins by Lectin Blot Analyses*—We compared the oligosaccharide structures on biliary glycoproteins with those on serum glycoproteins by several types of lectin blot analyses. It has been reported that almost all of the serum proteins are detected in bile, but the volume of each protein might be different (14). As shown in Fig. 1*A*, the staining pattern with Coomassie Brilliant Blue R-250 was very similar between bile and serum proteins except for a few bands. As shown in Fig. 1*B*, enhanced intensities of AOL and AAL binding in biliary glycoproteins were observed over a wide range of molecular mass compared with those in serum glycoproteins. There were few changes in the SSA and MAM blot analyses, suggesting that the sialylation of biliary and serum glycoproteins was almost the same level. In the case of ConA blot analysis, the intensity of lectin binding was slightly higher in biliary glycoproteins than in serum glycoproteins. However, the differences were not prominent in comparison with AOL and AAL blot analyses. These results show that biliary glycoproteins contained many fucose residues that are recognized by AOL and AAL lectins compared with serum glycoproteins, whereas total oligosaccharide structures differed only slightly.

As shown in Fig. 1*C*, a slight increase in carbohydrate labeling by the ECL glycoprotein detection system (Amersham Biosciences) was observed in biliary proteins as compared with serum proteins, which was in accordance with a result of ConA blot analysis. This shows that the levels of glycoproteins were increased in bile compared with serum. Although these data might enhance the AOL and AAL lectin blots results, no dramatic changes were observed in the other lectin blots.

*Structural Analysis of PA Oligosaccharides from Human Biliary and Serum Glycoproteins*—As shown in Fig. 1, fucosylated glycoproteins might be selectively secreted into the bile. To determine the oligosaccharide structures on biliary and serum glycoproteins in more detail, two-dimensional mapping HPLC and MALDI-TOF MS analyses were performed. PA oligosaccharides from biliary and serum glycoproteins were separated by reverse phase HPLC (Fig. 2, *A* and *B*). Each peak was isolated and chromatographed by normal phase HPLC. The elution positions of each peak were recorded as glucose units (Table 1) and their structures were determined based on the glucose units (22). The structural assignments were supported by the MALDI-TOF MS analyses (Table 1) and digestion with $\alpha$-fucosidase and $\beta$-galactosidase (data not shown). As shown in Fig. 2*C*, the percentages of peaks 5, 8, and 10 in fucosylated oligosaccharides on biliary glycoproteins were larger than those on serum glycoproteins. These results indicate that both $\alpha$1–3 (peak 5) and $\alpha$1–6 (peaks 8 and 10) linkages of fucose residues were increased in biliary glycoproteins.

*The Comparison of Oligosaccharide Structures on Hepatic Glycoproteins Purified from Human Bile and Serum*—To gain a better understanding of the fucosylation levels of a liver-specific protein in bile and serum, we analyzed the oligosaccharide structures on AAT, Hp, and AGP purified from bile and serum. AAT, Hp, and AGP are major serum glycoproteins that are produced mainly in the liver and possess three, four, and five *N*-glycans, respectively. As shown in Fig. 3, all of these hepatic glycoproteins purified from bile showed much higher reactivities to the AOL and AAL lectins than those purified from serum. These results were consistent with data for lectin blot analysis on total glycoproteins in bile and serum. The difference in AAT between bile and serum was not due to *N*-glycosylation but to the peptide moiety. The *N*-terminal sequence of biliary AAT revealed that 16 amino acid residues were removed from the *N*-terminals.

We next analyzed the oligosaccharide structures on hepatic glycoproteins by HPLC analysis in more detail. As shown in Fig. 4, the levels of both $\alpha$1–3 and $\alpha$1–6 fucosylated oligosaccharides in AAT, Hp, and AGP purified from bile were increased to a greater extent than those purified from serum.

*Fractionation of Human Biliary and Serum AGP by AOL Lectin Affinity Chromatography*—As shown in Figs. 1–4, glycoproteins in bile were strongly fucosylated compared with those in

Downloaded from www.jbc.org at OSAKA UNIVERSITY on April 8, 2007